

~~CONFIDENTIAL~~

Copy 5
RM L51F27

NACA RM L51F27

c.1

SEP 10 1951
NACA

RESEARCH MEMORANDUM

WATER LANDING INVESTIGATION OF A HYDRO-SKI MODEL
AT BEAM LOADINGS OF 18.9 AND 4.4

By Sidney A. Batterson

Langley Aeronautical Laboratory
Langley Field, Va.

CLASSIFICATION CANCELLED

FOR REFERENCE

Authority *NACA R7 3032* Date *7/20/53*

By *mdf* *8/11/53* See _____

NOT TO BE TAKEN FROM THIS ROOM

CLASSIFIED DOCUMENT

This document contains classified information affecting the National Defense of the United States within the meaning of the Espionage Act, USC 5031 and 32. Its transmission or the revelation of its contents in any manner to an unauthorized person is prohibited by law.
Information so classified may be imparted only to persons in the military and naval services of the United States, appropriate civilian officers and employees of the Federal Government who have a legitimate interest therein, and to United States citizens of known loyalty and discretion who of necessity must be informed thereof.

NATIONAL ADVISORY COMMITTEE FOR AERONAUTICS

WASHINGTON
September 12, 1951

~~CONFIDENTIAL~~



NATIONAL ADVISORY COMMITTEE FOR AERONAUTICS

RESEARCH MEMORANDUM

WATER LANDING INVESTIGATION OF A HYDRO-SKI MODEL

AT BEAM LOADINGS OF 18.9 AND 4.4

By Sidney A. Batterson

SUMMARY

Water landing tests were made in the Langley impact basin with a model having a flat rectangular planing surface together with a pulled-up bow and a simulated landing wheel. The majority of the test runs were made in smooth water; however, three landings were made in waves approximately $1\frac{1}{3}$ feet high by 30 feet long. The trim range varied from 0° to 15° and the flight-path angle ranged from approximately 2° to 20° . Runs were made at beam loadings of 18.9 and 4.4. The results are presented as plots showing the variation of the nondimensional loads and motions with both the wetted length and flight-path angle. It was concluded that the results could be used to approximate the load and motion values for the practical range of beam loadings. The experimental results indicated that the effect of the landing wheel was small; in addition, the experimental results yielded quantitative load values resulting from immersion of the pulled-up bow.

INTRODUCTION

As a result of current interest in the utility of skis as an all-purpose landing device for airplanes, an investigation has been undertaken by the NACA toward improvement in the design of these devices. Water landing tests were conducted in the Langley impact basin on a model having a flat rectangular planing surface together with a pulled-up bow and a simulated landing wheel. The primary purpose of these tests was to obtain the hydrodynamic impact loads during landing.

The majority of the test runs were made in smooth water; however, three landings were made in waves approximately $1\frac{1}{3}$ feet high by 30 feet long. The trim range varied from 0° to 15° and the flight-path angle



ranged from approximately 2° to 20° . Runs were made at beam loadings of 18.9 and 4.4. The results obtained during this investigation were in urgent demand and, therefore, only 3 months was allotted between the start of initial preparations for testing and completion of this paper. This paper, therefore, does not contain a detailed analysis of the findings but, however, does present the test results and shows the effects of various parameters.

SYMBOLS

b	model beam, feet
F	hydrodynamic force, pounds
\dot{f}	equivalent planing velocity, feet per second ($\dot{x} + \dot{y} \cot \tau$)
M	pitching moment about axis "a", foot-pounds (see fig. 4)
n_{1w}	impact load factor, measured normal to undisturbed water surface, g units
p	unit bottom pressure, pounds per square inch
t	time, seconds
V	resultant velocity, feet per second
W	dropping weight, pounds
w	specific weight of water (62.4 lb/cu ft)
\dot{x}	velocity of model parallel to undisturbed water surface, feet per second
y	immersion of model normal to undisturbed water surface, feet
\dot{y}	velocity of model normal to undisturbed water surface, feet per second
γ	flight-path angle (referred to undisturbed water surface), degrees
λ	distance from model step (parallel to flat bottom surface of model), beams

ρ density of water (1.938 slugs/ft³)
 τ model trim (referred to undisturbed water surface), degrees

Subscripts:

k parallel to flat bottom surface of model
 max maximum
 n normal to flat bottom surface of model
 o at water contact
 p to peak pressure line

Dimensionless variables:

C_{Δ} beam-loading coefficient $\left(\frac{W}{wb^3}\right)$

C_n normal-force coefficient $\left(\frac{F_n}{\frac{1}{2} \rho V_o^2 b^2}\right)$

C_D draft coefficient $\left(\frac{y}{b}\right)$

C_{d_k} drag coefficient parallel to flat bottom surface of model
 $\left(\frac{F_k}{\frac{1}{2} \rho V_o^2 b^2}\right)$

C_M pitching-moment coefficient $\left(\frac{M}{\frac{1}{2} \rho V_o^2 b^3}\right)$

$C_{l_{\max}}$ maximum lift coefficient $\left(\frac{(n_{l_w})_{\max} W}{\frac{1}{2} \rho V_o^2 b^2}\right)$

$\frac{\dot{y}}{\dot{y}_0}$ vertical velocity ratio

C_p pressure coefficient $\left(\frac{p}{\frac{1}{2} \rho v^2} \right)$

APPARATUS

The investigation was conducted in the Langley impact basin with the test equipment described in reference 1. The basic model used for these tests was described in reference 2. Two distinct configurations of this model were tested, one at a beam loading of 18.9 and the other at a beam loading of 4.4. For the heavy-beam-loading condition the basic model was modified to the extent of adding a pulled-up bow and a simulated landing wheel. For the light-beam-loading conditions the beam was increased 8 inches by addition of 4-inch structural steel angles to each side of the basic model. The simulated landing wheel was removed for all test runs made in the light-beam-loading condition. The lines and pertinent dimensions corresponding to both configurations are shown in figure 1. Figures 2 and 3 are photographs of the model mounted for testing in the heavy-beam-loading configuration and in the light-beam loading configuration, respectively. The model was attached to a dynamometer which in turn was rigidly attached to the carriage boom. Variations in trim were obtained as described in reference 2 by utilizing various length of trim links between the rear attachment point of the dynamometer and boom.

The instrumentation used to measure both the vertical displacement and velocity and the horizontal velocity was described in reference 1. Accelerations in the vertical direction were measured by an oil-damped unbonded strain-gage type of accelerometer having an undamped natural frequency of 105 cycles per second. The galvanometer used to record the accelerometer output had a natural frequency of 100 cycles per second and the combination of accelerometer and galvanometer was adjusted to yield an over-all damping value of approximately 65 percent of the critical damping. The hydrodynamic forces normal and parallel to the model bottom were measured by the dynamometer. This same dynamometer yielded values of pitching moment about an athwartship axis through "a" (fig. 4). The initial contact of the model with the water was determined by means of an electrical circuit completed by the water. Unit bottom pressures were measured with 12 pressure gages located in the model bottom as shown in figure 5. The pressure gages had flat $\frac{1}{2}$ -inch-diameter

clamped-edge diaphragms mounted flush with the model bottom. Natural frequencies of the pressure gages exceeded 2000 cycles per second and the natural frequencies of the galvanometers were in the neighborhood of 1600 cycles per second. The combination of gage and galvanometer was adjusted to yield an over-all damping value of approximately 65 percent of the critical damping. Complete time histories of the values of the quantities measured with the above instrumentation were obtained on a single multichannel recording oscillograph.

For the runs with waves, wave profiles were obtained from an instrument mounted in the impact basin structure approximately 100 inches above the undisturbed water surface. This instrument consisted of a light source and lens system which projected a vertical parallel beam of light, several inches in diameter, onto the water. The spot of light on the water surface was photographed on a moving film located in a film drum at an angle to the vertical. The film drum was located about 4 feet horizontally from the light source, and the plane formed by the light beam and line of sight of the film drum opening was perpendicular to the longitudinal center line of the tank. Fluorescin dye was introduced into the water in order to intensify the light spot and thus obtain a readable record line on the film. The impulse from a common switch closed by the carriage during the test run was recorded on both the oscillograph record and wave profile record. Since both recorders were equipped with timers this common impulse served to correlate both records. The wave length was adjusted to 30 feet and maintained constant prior to each run.

TEST PROCEDURE

The model was tested at trims of 0° , 3° , 6° , 9° , 12° , and 15° . The horizontal velocity for these tests ranged from approximately 30 feet per second to 90 feet per second, and the initial vertical velocity ranged from approximately 2 feet per second to 10 feet per second. The depth of immersion of the model was measured from the instant of initial water contact and in a direction perpendicular to the undisturbed water surface. Throughout the immersion a lift force equal to the total weight of the model and drop linkage was exerted on the model by means of the lift engine described in reference 1.

Tests were made at beam loadings of 18.9 and 4.4. The total dropping weight was 1180 pounds in the heavy-beam-loading condition. Addition of the side angles to the model for the light-beam-loading condition increased the total dropping weight to 1260 pounds. Actual instantaneous wetted lengths, as defined by the distance from the model step to the point of peak pressure, were determined by noting the instant of the initial peak exhibited by each pressure gage. Since the location

of each gage was known, the instant at which each gage peaked determined the wetted length at that instant.

The model together with the drop linkage weighed 1180 pounds; however, they were in turn attached to a carriage weighing 5400 pounds. This condition had some effect on the motion of the model in that the drag forces acting on the model did not develop the horizontal acceleration that would have resulted in the absence of the carriage mass.

RESULTS AND DISCUSSION

The instantaneous value of the transient load occurring on a flat rectangular surface upon impact with a smooth water surface is primarily a function of the initial velocity and instantaneous values of the trim, flight-path angle, and draft. However, other effects such as instantaneous acceleration serve in some degree to attenuate the load. The effect of velocity is known and can be eliminated from the results by choice of a suitable coefficient provided that the initial velocity is sufficient to make Froude effects negligible. All test results contained in this paper were derived from runs made at sufficiently high speeds so that Froude effects have no practical significance. The investigation was made at fixed trims, that is, the model trim referred to the undisturbed water surface remained constant throughout the immersion. No attempt was made to eliminate the effect of trim in the presentation of the results. The instantaneous flight-path angle and draft are affected appreciably by the beam loading. This fact must be taken into account when using the results contained in this paper for the determination of design loads for skis having beam loadings different from those tested. It should be noted that skis with pointed steps are outside the scope of this investigation. The effect of beam loading upon flight-path angle stems from the fact that separate landings, which are made with initial conditions that are identical except for beam loading, will yield accelerations normal to the impacting surface that are different. The landings made at the lower beam loadings will exhibit larger accelerations. This results in a higher rate of decrease of the vertical velocity for the light-beam-loading condition under the existing test conditions at the impact basin in which the horizontal velocity remains substantially constant. It then follows that, since the vertical velocity time history is a function of the beam loading, the draft, the flight-path angle, and, therefore, the load time history will also be affected by the beam loading.

It was felt that the most effective data presentation would be achieved by plotting the experimental load and motion variables converted to nondimensional coefficients against wetted length in beams

as a parameter. The wetted length λ_p is defined as the distance (in beams) from the model step to the line of peak pressure on the model bottom.

Figures 6, 7, and 8 show the variation of the nondimensional coefficients of normal load, pitching moment, and vertical velocity with the nondimensional wetted length for $C_\Delta = 18.9$. The initial flight-path angles γ_0 are noted by the symbols accompanying each curve. In some cases the difference between initial flight-path angles is small enough so that one curve is sufficient to fair both sets of points. The values of λ_p appearing in the figures for the bow region of the model are obtained by projecting the point of peak pressure on the bow normal to the extended straight portion of the model bottom; in terms of λ_p the bow extends from 5 to 6.16 for the model with $C_\Delta = 18.9$ and from 3 to 3.7 for the model with $C_\Delta = 4.4$ (no data are presented subsequent to the inception of bow immersion for the light-beam-loading conditions).

In order to obtain data on the beam-loading effect, the model beam was increased 8 inches changing the C_Δ value from 18.9 to 4.4, and a series of runs was made at trims of 3° , 9° , and 15° . Figures 9, 10, and 11 present the data obtained from these runs plotted in coefficient form against the wetted length in beams. Figures 6, 7, 8 and 9, 10, and 11 can be compared directly for the same trims and initial flight-path angle to obtain the effect of beam loading on load, moment, vertical velocity, and draft since the ordinates and abscissas are in nondimensional form. A comparative examination of these figures reveals that although the beam loading was changed by a factor of 4.3, the change in the nondimensional load moment and maximum draft was only of an order of approximately 2. Since the change in the coefficients is appreciably slower with respect to changes in beam loading, it is felt that plots similar to those presented in figures 6, 7, 8 and 9, 10, and 11 could be made up with reasonable accuracy for other beam loadings by interpolation between curves. It should be borne in mind that such curves would be valid only for surfaces having a rectangular plan form. It would have been desirable to obtain more detailed results on the effect of beam loading by extending the investigation; this, however, was prevented by lack of time.

Since the horizontal velocity remained approximately constant throughout the impact, figures 8 and 11 can be considered as showing the variation of flight-path angle with wetted length. Furthermore, by selecting values of C_n from figures 6 and 9 at even beam lengths, that is, 1, 2, 3, and so forth, and noting the corresponding instantaneous flight-path angle from figures 8 and 11, the variation of normal-load coefficient with instantaneous flight-path angle can be obtained for the aspect ratios 1, 2, 3, and so forth. Figures 12 and 13 present this

cross plot. It can be noted in figure 12 that as the aspect ratio increases the faired lines fall closer together; in fact, the aspect ratios of 4 and 5 are faired by a single line. Extrapolation of the faired lines through the test points to $\gamma = 0$ should yield a fair check with the planing value. This check should be closer for the runs made at $C_{\Delta} = 18.9$ since reduction in vertical load resulting from acceleration of the virtual mass will be less apparent at the high beam loadings. A quantitative measure of the load reduction due to acceleration of the virtual mass can be obtained by comparing values of C_n appearing in figures 12 and 13 at corresponding trims, aspect ratios, and flight-path angles.

Figure 14 shows the variation of $C_{n_{max}}$ with initial flight-path angle for both beam loadings. The trend appears to be independent of trim. In connection with figure 14 it should be pointed out that $F_{n_{max}}$ occurred prior to the beginning of bow immersion for all test runs made in smooth water.

Figure 15 shows the variation of the maximum draft coefficient with initial flight-path angle for beam loadings of 4.4 and 18.9. The faired line through the test points obtained from runs at the heavy beam loading is taken from reference 2. Apparently, when maximum draft occurs prior to bow immersion the same variation (unflaged points) is obtained as in reference 2. This is to be expected since the conditions were practically identical except for addition of the simulated landing wheel. However, for initial flight-path angles greater than 9° in which the bow was immersed the test points fall below the curve established for runs in which no bow immersion occurred. This indicates a smaller draft value than would have been attained had the bottom continued straight and is attributed to an increase in lift due to immersion of the bow. It can be noted further that during two runs made at low flight-path angles and at trims of 3° and 6° , in which the bow entered the water, the test points fall above the curve, larger drafts thereby being indicated than would have been attained in the absence of bow immersion. This is probably due to the presence of an area just aft of the bow exhibiting pressures lower than would occur in the absence of a pulled-up bow. Such a phenomenon apparently occurs at the low trims and low flight-path angles and might be considered to result from the downwash imparted to the water by the bow.

Figure 16 shows the variation of maximum lift coefficient with initial flight-path angle for $C_{\Delta} = 18.9$ and $C_{\Delta} = 4.4$. The dashed line appearing in figure 16 was obtained from reference 2 for $C_{\Delta} \approx 18.9$, and shows excellent agreement with the test points obtained during this investigation. This indicates that the same relationship between maximum vertical acceleration and initial flight-path angle was obtained during both investigations.

Figure 17 shows the variation of the drag coefficient parallel to the model bottom with wetted length. The dynamometer struts used to measure drag load were always parallel to the straight portion of the model bottom and therefore measured only the load in this direction. Since the model had a certain amount of mass, the drag load obtained from the dynamometer had to be corrected for the inertia component of the model in the drag direction in order to isolate the hydrodynamic load. This was accomplished by noting the vertical accelerometer readings at the desired instant and applying a suitable correction based on the model mass and trim. It is apparent that, within the limits of accuracy obtainable with this dynamometer, the drag load coefficient is zero for the straight portion of the model. The scatter which in some cases results in negative values is attributed to the combined reading and instrument errors from the dynamometer and accelerometer.

Figures 18 and 19 show the variation of pressure coefficient with length for various wetted lengths and trims, where the sequence of plots at each trim corresponds to increased values of wetted length. Figure 18 contains results obtained at $C_{\Delta} = 18.9$ and figure 19 the results obtained at $C_{\Delta} = 4.4$. The trim values used in determining the equivalent planing velocity ($\dot{f} = \dot{x} + \dot{y} \cot \tau$) for the bow pressure gages was the actual angle made by the flat pressure-gage diaphragm with the undisturbed water surface. As the trim is reduced the areas of peak pressure become highly localized. This results in lower peak pressure recordings as the pressure area becomes small compared to the gage size. This effect becomes very pronounced at 3° trim and is apparent at 6° and 9° trim. It is possible that in addition to the gage-size effect some of the attenuation of the pressure peaks might be a result of the frequency response characteristics of the pressure gage and recording galvanometer combination. The fairing of the curves was based on time histories of the pressure records obtained for the highest flight-path-angle impact at each trim. No attempt was made to fair the 3° trim runs since the attenuation of the peaks was so great. Also no attempt was made to fair the points obtained from the bow pressure gages since, at the same instant of time, the equivalent planing velocity was a variable between adjacent pressure-gage locations owing to the varying trim in this region. A comparison of the pressure coefficients obtained from runs made at $C_{\Delta} = 4.4$ with those obtained at $C_{\Delta} = 18.9$ shows that the sustained pressure over the straight portion of the model bottom are lower for $C_{\Delta} = 4.4$ due to load reductions which result from greater accelerations of the virtual mass at the lighter beam loadings. However, in the step region the peak pressure coefficients are higher for the light-beam-loading condition, sometimes exceeding one. This is explained by the fact that the beam is greater for the light-beam-loading condition but the actual distance of the pressure gages from the step is the same as in the heavy-beam-loading condition. Therefore, the distance to the step measured in beams for the same gages is less for runs made at

$C_{\Delta} = 4.4$. As a result, the increase in pressure due to rate of water rise as discussed in reference 3 is greater for the same gages in the region of the step for runs made at $C_{\Delta} = 4.4$. The fact that the pressure-gage area was the same for both conditions, although the beam was increased, may also contribute to obtaining higher pressure coefficients during the test runs made at $C_{\Delta} = 4.4$.

The size of the simulated landing wheel was based on measurements made on the ski used on the L-5 airplane. By noting the axle center line and the size and shape of the cutout in the ski, the wheel size and shape was constructed. The full-size wheel was scaled to one-half size for these tests since the test model had a beam of approximately one-half the actual ski beam in the region of the wheel. This scaling satisfied the condition of similitude so that results obtained relative to the wheel from these model tests are applicable to the L-5 ski.

The effect of the simulated landing wheel appears to be negligible from the standpoint of over-all loads. It was previously noted that for runs with the wheel in place the drag load parallel to the model bottom over the straight bottom portion was too small to be measured by the dynamometer (fig. 17). Furthermore, the lift coefficient obtained with the wheel in place was identical with that obtained in the absence of a wheel (fig. 16). Examination of the bottom pressure records showed the wheel effect to be greatly localized. The only pressure gage apparently showing effects of the wheel was number 2; however, on several runs made at low trims, some effect was noted on pressure gages 1 and 11. It was noted that as the flight-path angle increased pressure gage 2 showed smaller interference effects due to the wheel. The effect of the wheel on the pressure gages was evidenced by erratic changes in pressure with time together with considerable reduction in the initial peak pressure. In some cases no definite initial peak was recognizable.

One smooth water run was made at a trim of 0° . The nondimensional coefficients are plotted against time in figure 20. Figure 21 shows the actual value of the bottom pressures plotted against time for this run. The actual pressures are presented since the pressure coefficients which are based on the equivalent planing velocity would yield no information for the 0° trim case (since for $\tau = 0$, $\cot \tau = \infty$). Examination of figure 21 shows that several of the pressure gages on the aft portion of the bottom were wetted before the remaining forward ones on the straight portion of the bottom. This is attributed to disturbances present on the water surface induced by air motion created by the carriage and by the model as it neared the water surface.

Three runs were made in rough water, two at 0° trim and one at 3° trim. Figure 22 shows the variation of wave height to wave length for each run together with a sketch of the model made to the same scale

as the wave scale. The model is positioned on the wave at the initial point of contact. A wave velocity of approximately 11 feet per second was obtained from the wave profile record by noting the elapsed time between wave crests. The wave form obtained was not the optimum possible with the impact basin equipment, since this equipment was designed for operation with an 8-foot water depth in the basin. However, for this particular model it was necessary to make the rough-water runs in 6 feet of water. This reduced the effectiveness of the beaches and resulted in the wave shapes being subjected to reflections having larger magnitudes than is normal with this equipment. The nondimensional load and motion coefficients obtained during the rough-water runs are plotted against time in figures 23, 24, and 25. The actual values of pressure obtained during these runs are plotted against time in figures 26, 27, and 28. In all these figures, zero time denotes the instant of water contact.

It is possible to obtain some idea of the magnitude and character of the drag loads resulting from bow immersion by examination of the drag-load-coefficient time histories appearing in figures 20, 23, 24, and 25. The drag time history can be correlated to the location of the water line on the bow by noting the times at which the various bow gages are wetted.

In order to provide for the greatest utilization of the test data obtained during this investigation, table I was prepared containing the values of the independent parameters together with the corresponding experimentally obtained dependent parameters.

CONCLUDING REMARKS

The experimental results obtained during water landing tests of a 0° dead-rise model in the Langley impact basin are applicable in predicting the loads and motions exhibited by a flat rectangular ski during impact with a water surface. Although the investigation was made at beam loadings of 18.9 and 4.4, it is felt that the results can be used to approximate values for the practical range of beam loadings.

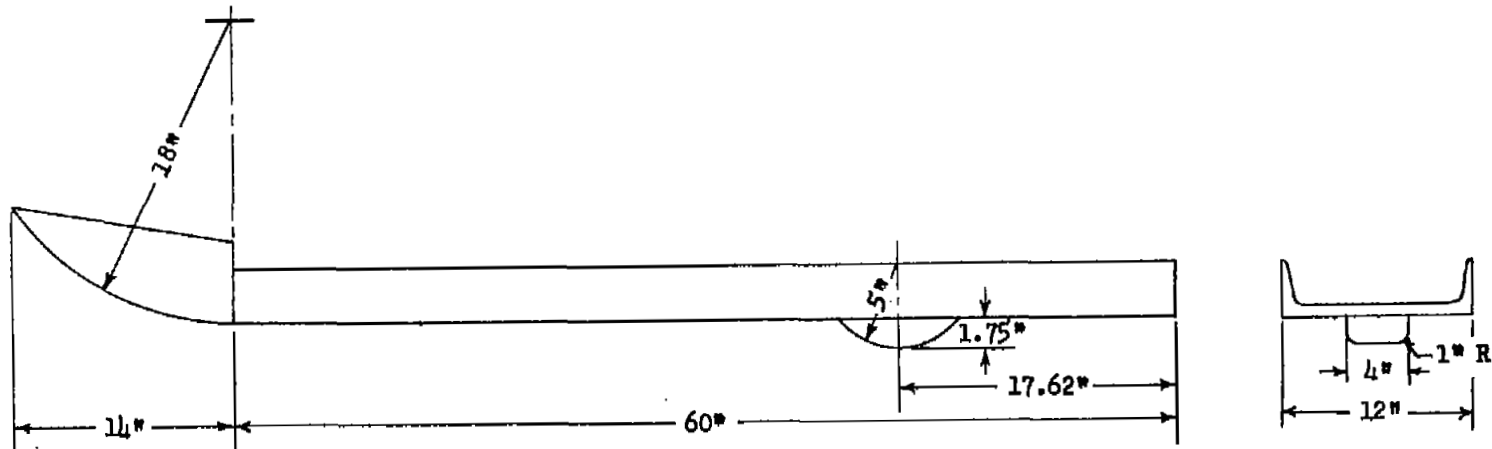
The experimental data indicated that the effect of the landing wheel on the ski used on the L-5 airplane was small from the standpoint of both drag and vertical acceleration.

It is felt that quantitative load values resulting from immersion of the bow can be determined from a study of the time histories presented of the three rough-water landings in addition to the run made in smooth water at 0° trim.

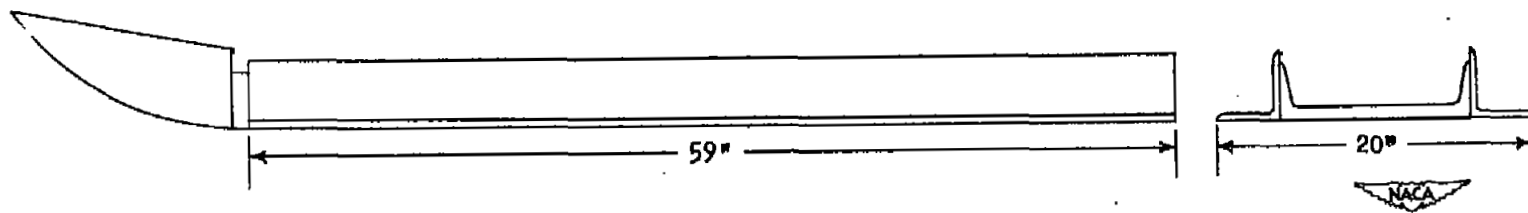
Langley Aeronautical Laboratory
National Advisory Committee for Aeronautics
Langley Field, Va.

REFERENCES

1. Batterson, Sidney A.: The NACA Impact Basin and Water Landing Tests of a Float Model at Various Velocities and Weights. NACA Rep. 795, 1944. (Formerly NACA ACR L4H15.)
2. McArver, A. Ethelda: Water-landing Investigation of a Model Having Heavy Beam Loadings and 0° Angle of Dead Rise. NACA TN 2330, 1951.
3. Smiley, Robert F.: An Experimental Study of Water-Pressure Distributions during Landings and Planing of a Heavily Loaded Rectangular Flat-Plate Model. NACA TN 2453, 1951.



Heavy-beam-loading configuration



Light-beam-loading configuration

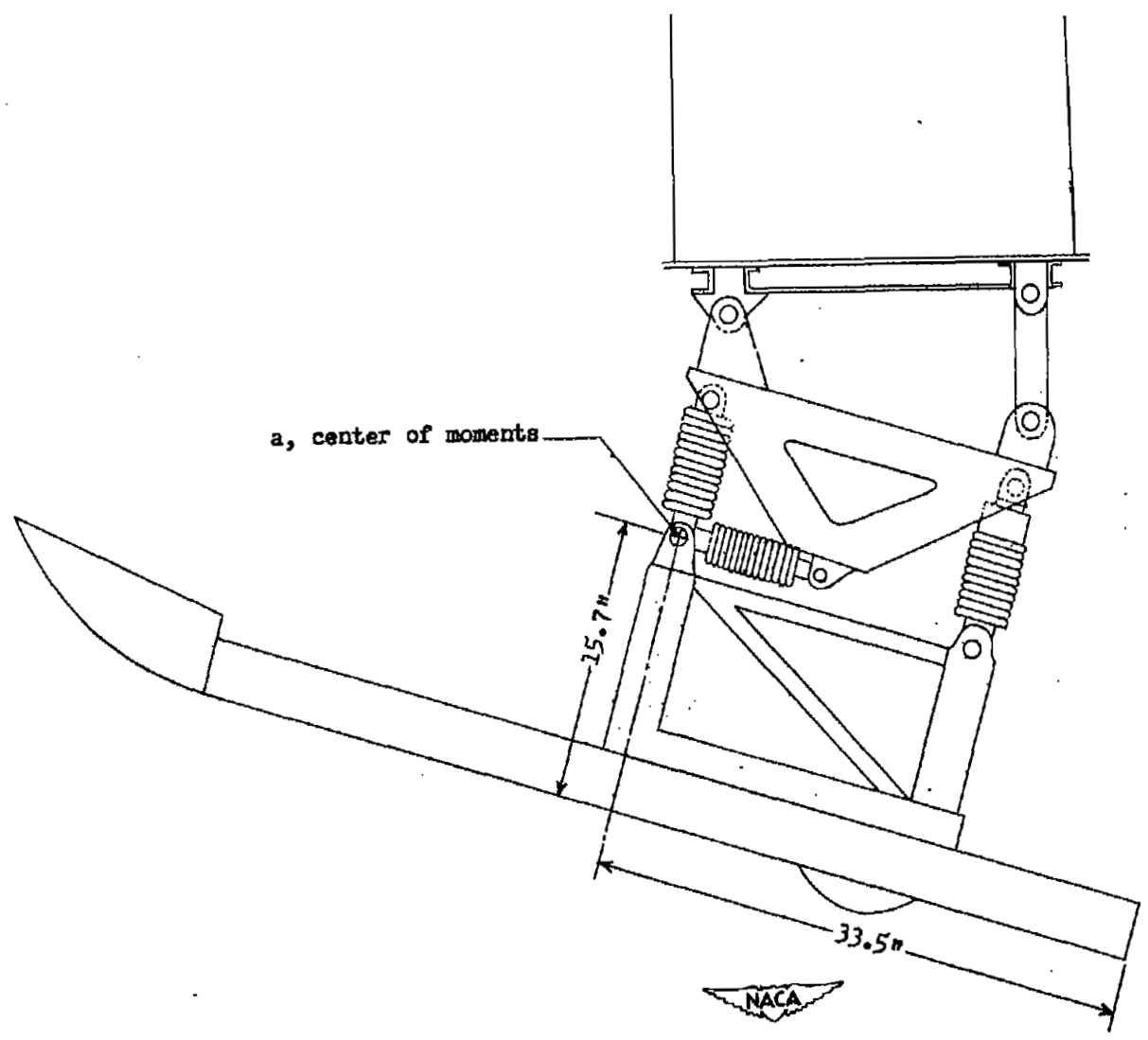
Figure 1.- Lines of 0° dead-rise model.



Figure 2.- Photograph of 0° dead-rise model mounted for testing in the heavy-beam-loading configuration.



Figure 3.- Photograph of 0° dead-rise model mounted for testing in the light-beam-loading configuration.



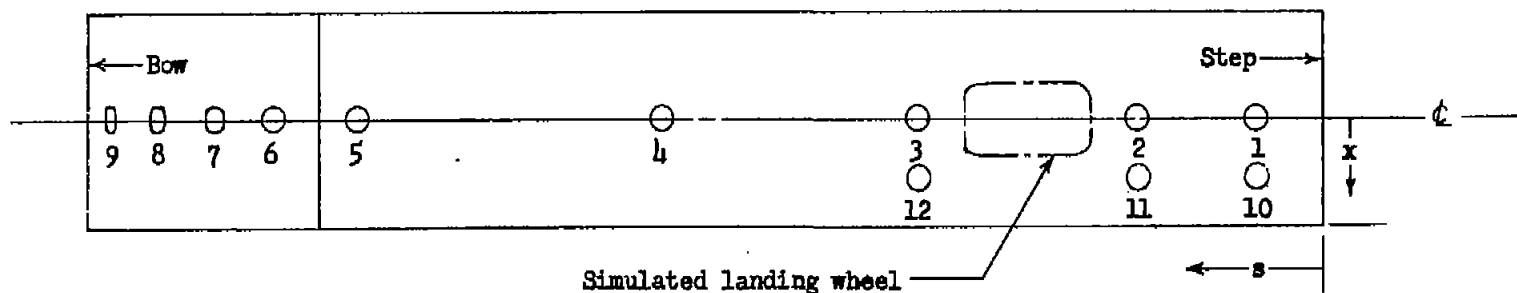
a, center of moments

15.7 in

33.5 in



Figure 4.- Location of pitching moment axis, a.



Position	s (in.)	x (in.)	Position	s (in.)	x (in.)
1	3.96	0	7	66.48	0
2	11.04	0	8	69.84	0
3	24.00	0	9	72.72	0
4	39.48	0	10	3.96	3.25
5	57.84	0	11	11.04	3.25
6	62.88	0	12	24.00	3.25



Figure 5.- Sketch showing pressure-gage locations on 0° dead-rise model.

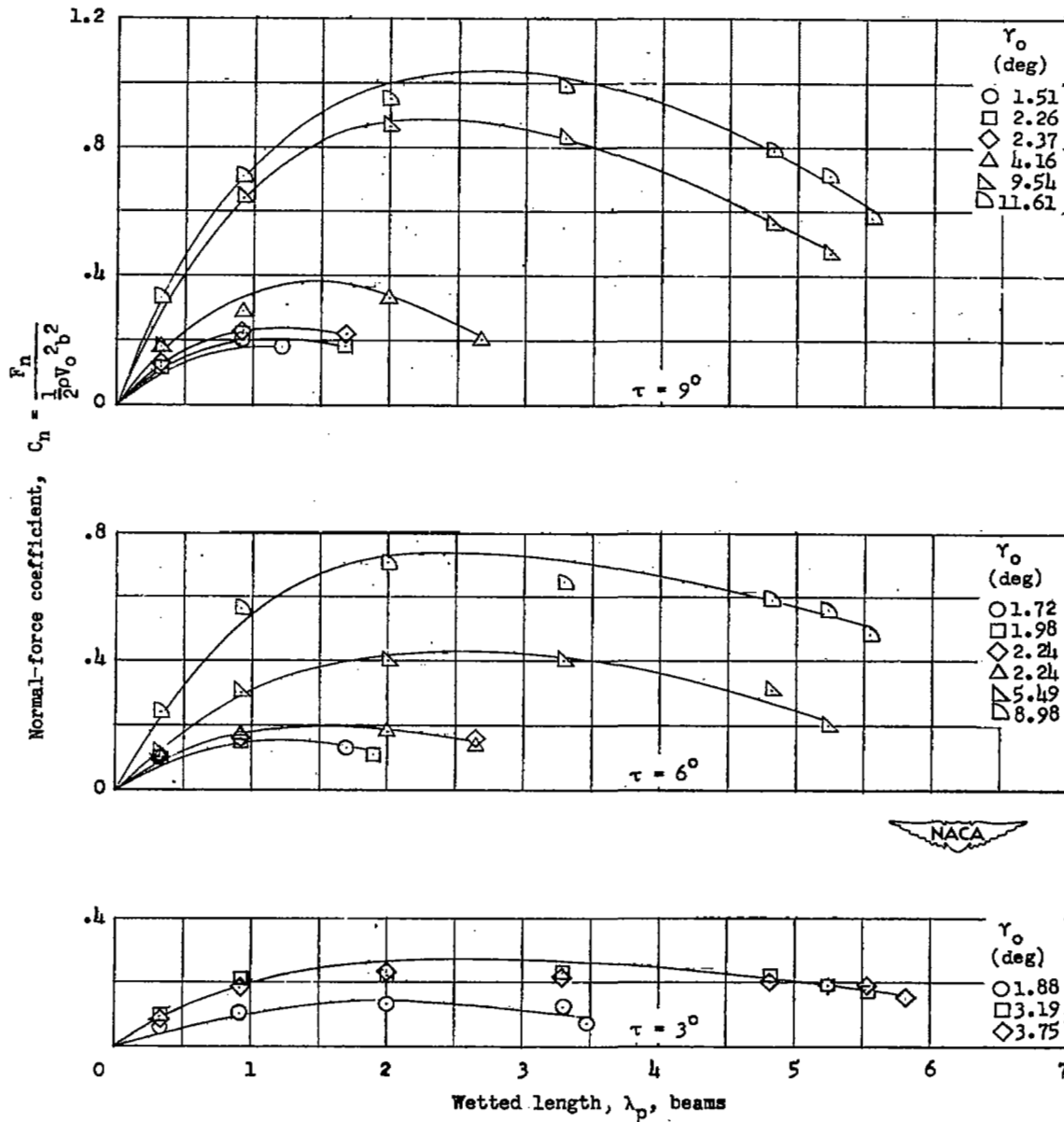


Figure 6.- Variation of normal-force coefficient with wetted length for various trims. $C_{\Delta} = 18.9$.

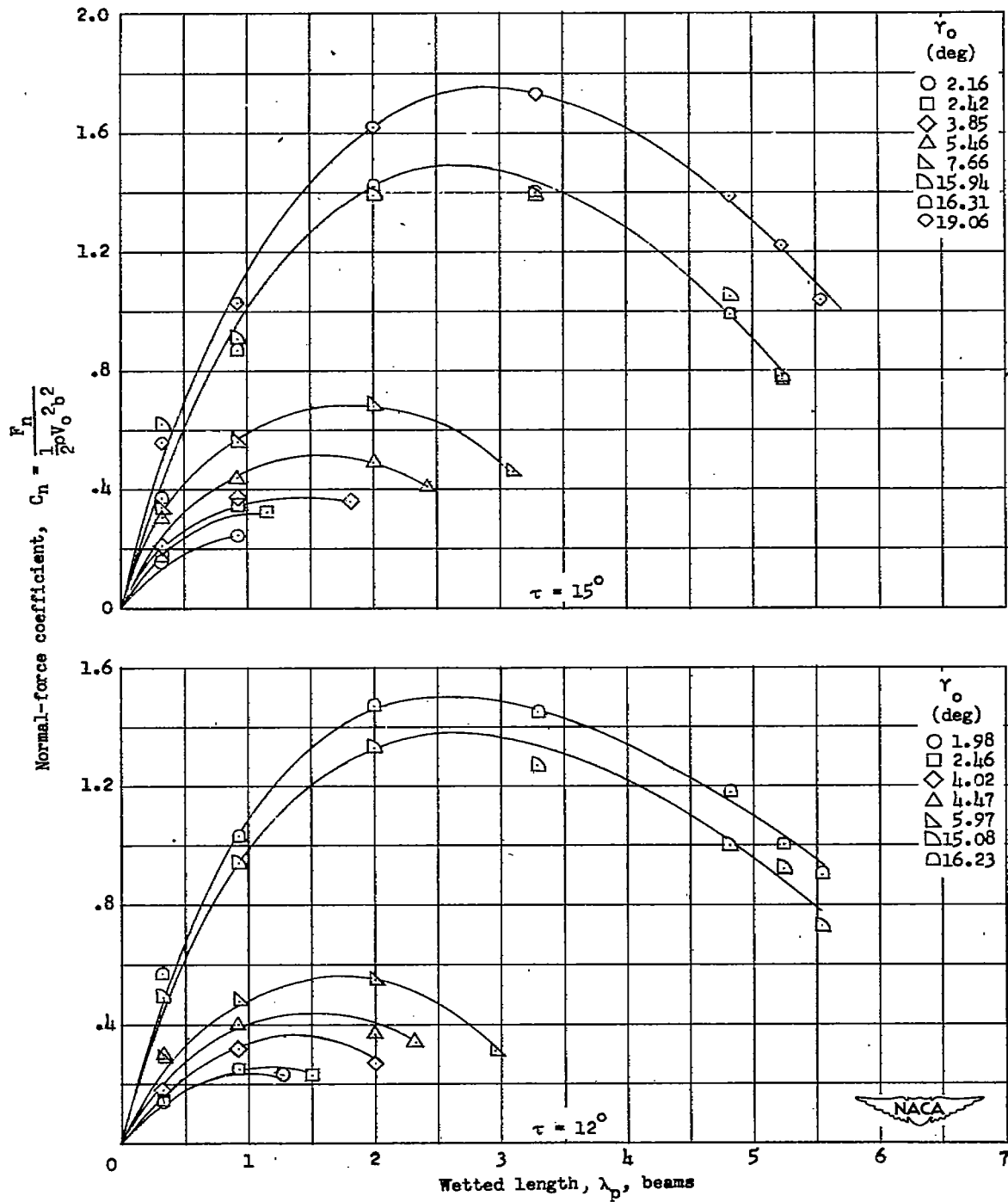


Figure 6.- Concluded.

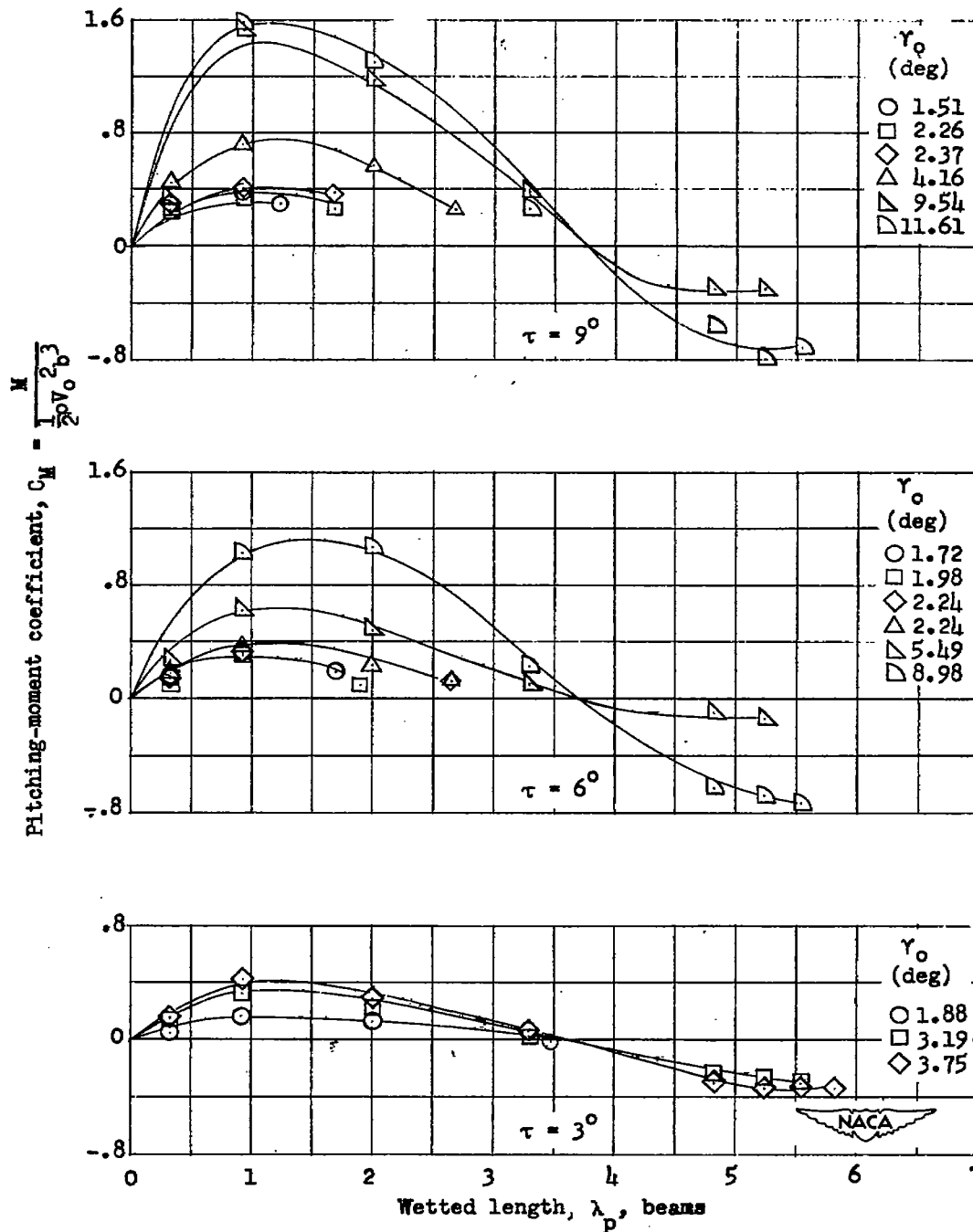


Figure 7.- Variation of pitching-moment coefficient with wetted length for various trims. $C_{\Delta} = 18.9$.

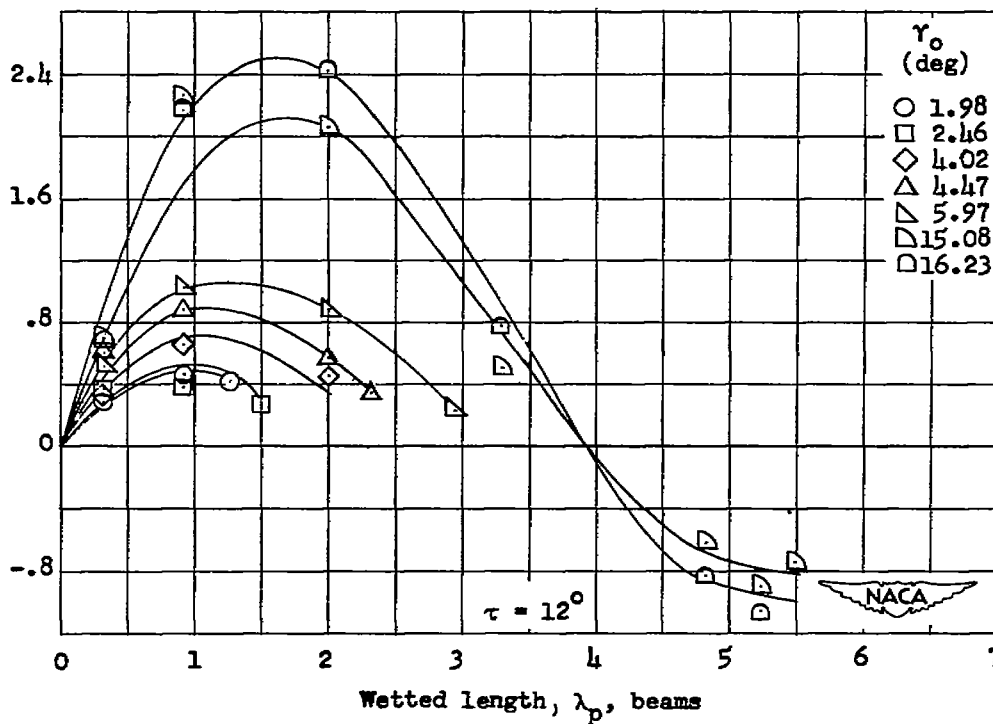
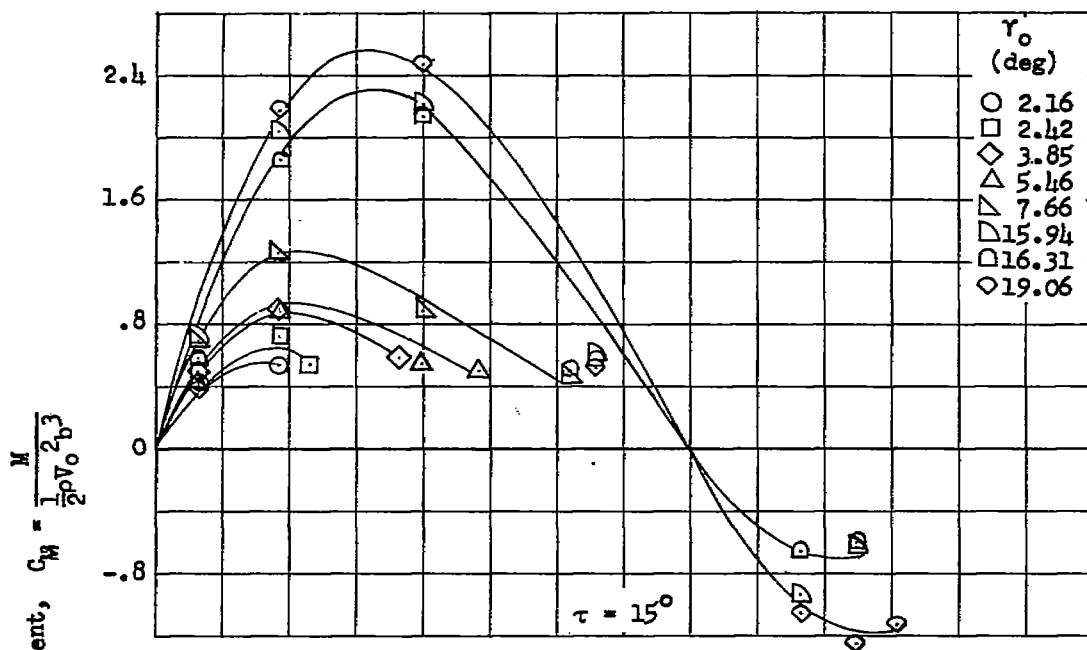


Figure 7.- Concluded.

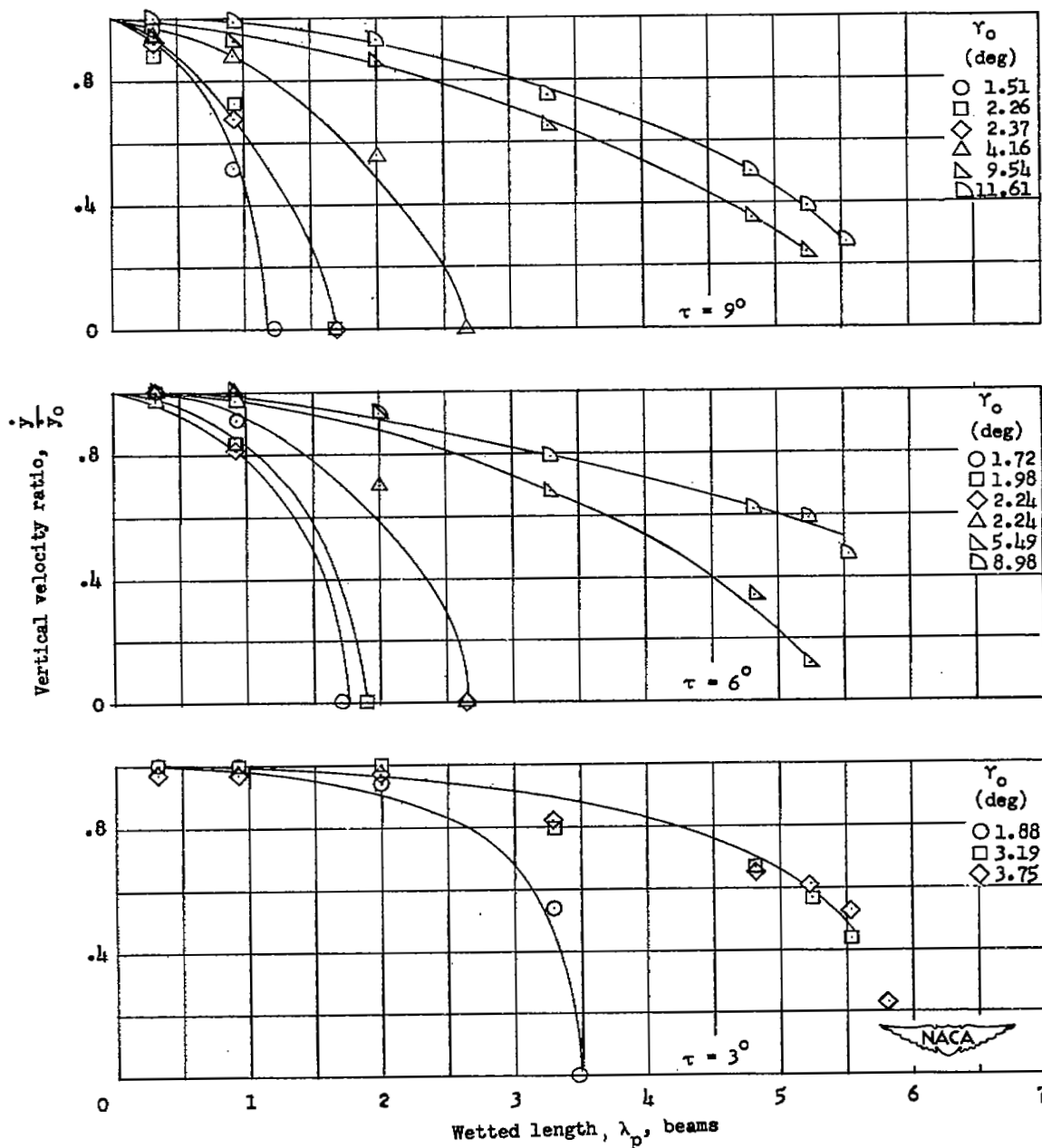


Figure 8.- Variation of vertical velocity ratio with wetted length for various trims. $C_{\Delta} = 18.9$.

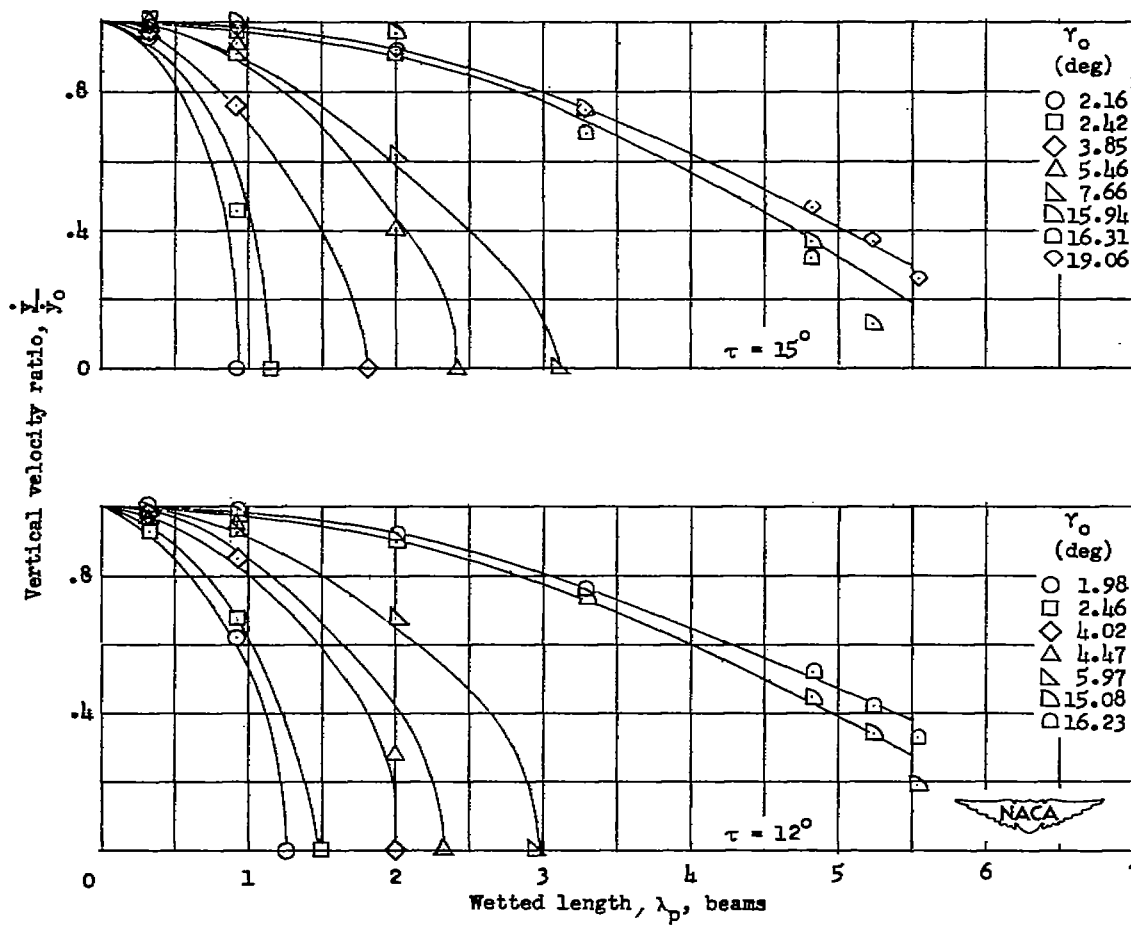


Figure 8.- Concluded.

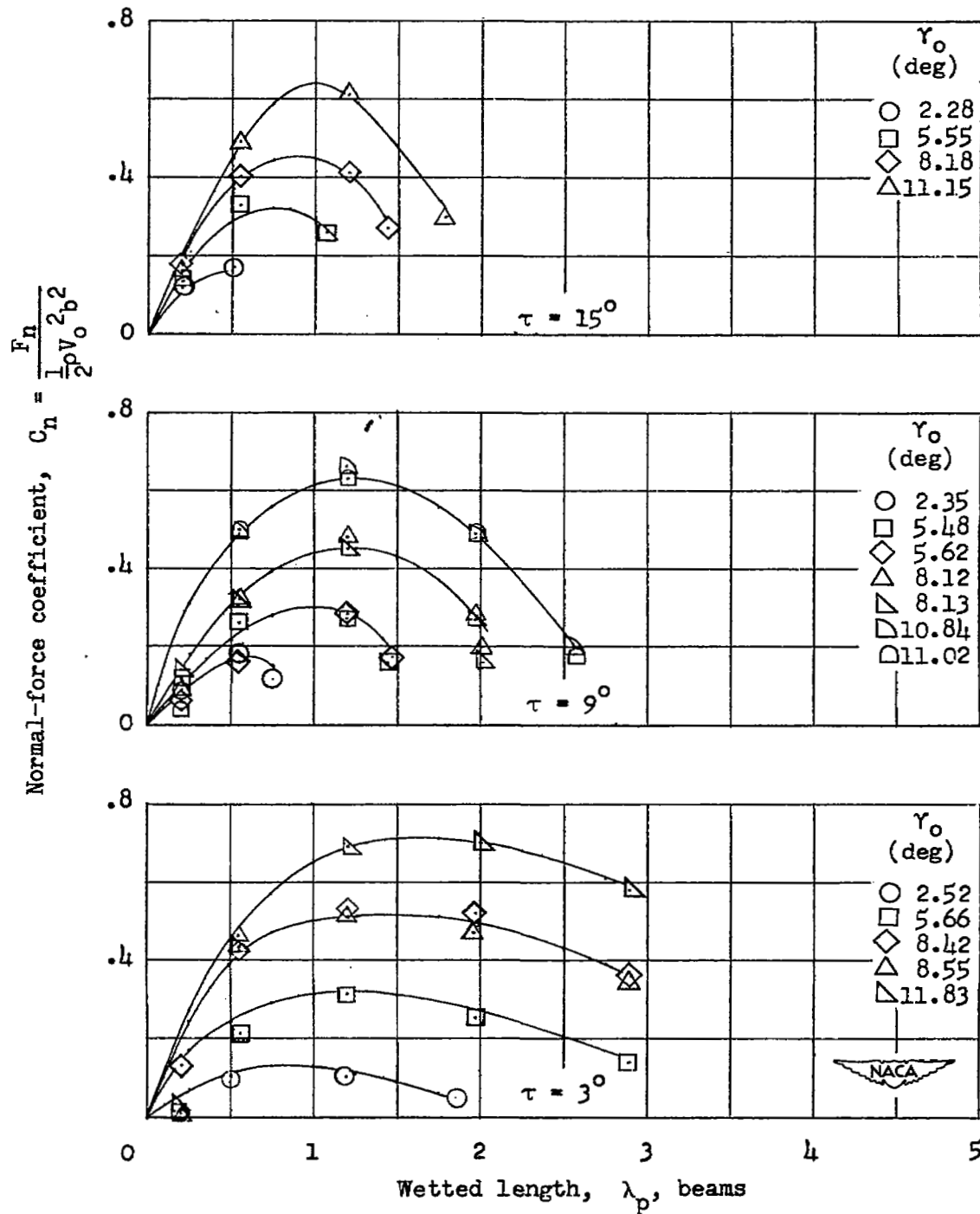


Figure 9.- Variation of normal-force coefficient with wetted length for various trims. $C_\Delta = 4.4$.

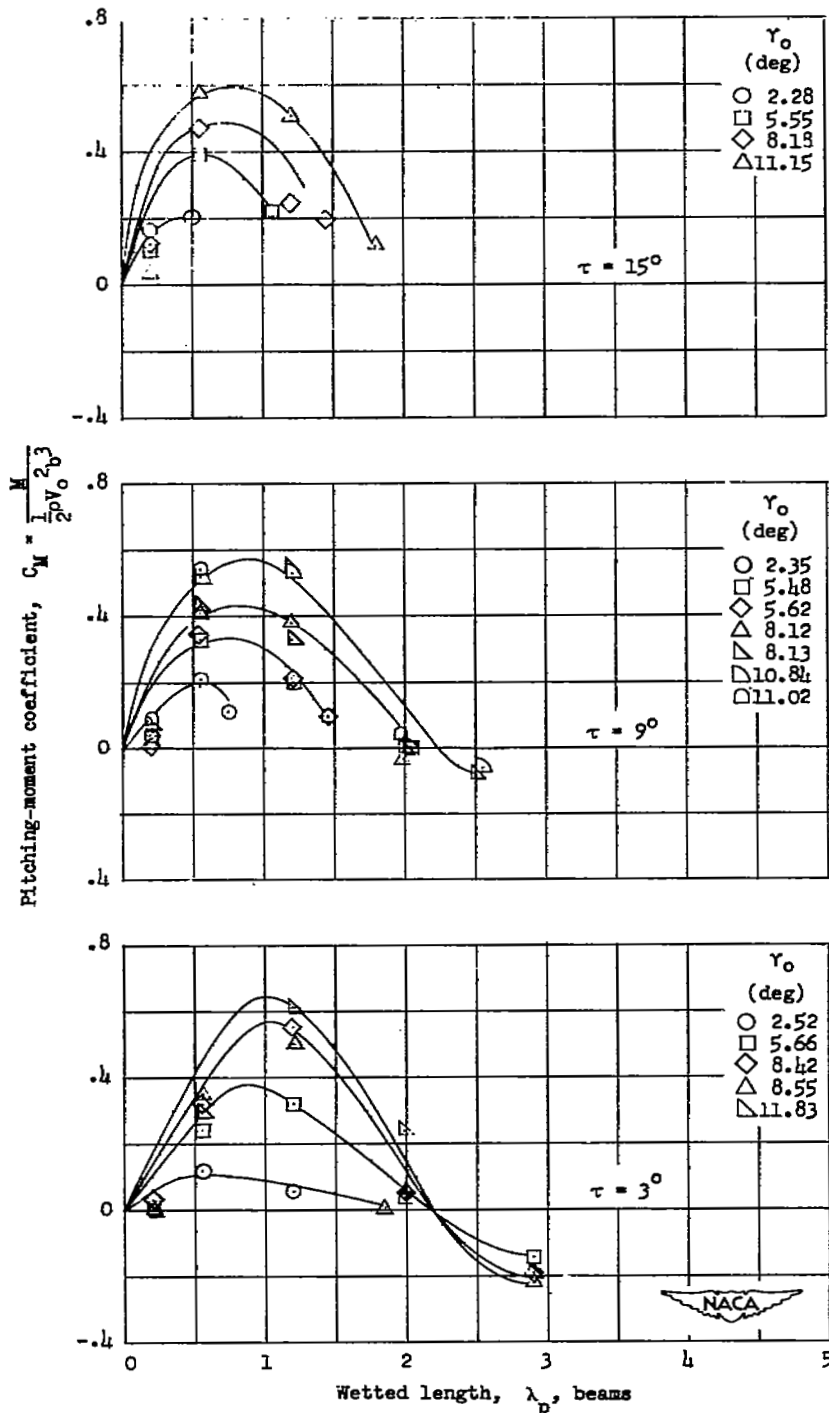


Figure 10.- Variation of pitching-moment coefficient with wetted length for various trims. $C_{\Delta} = 4.4$.

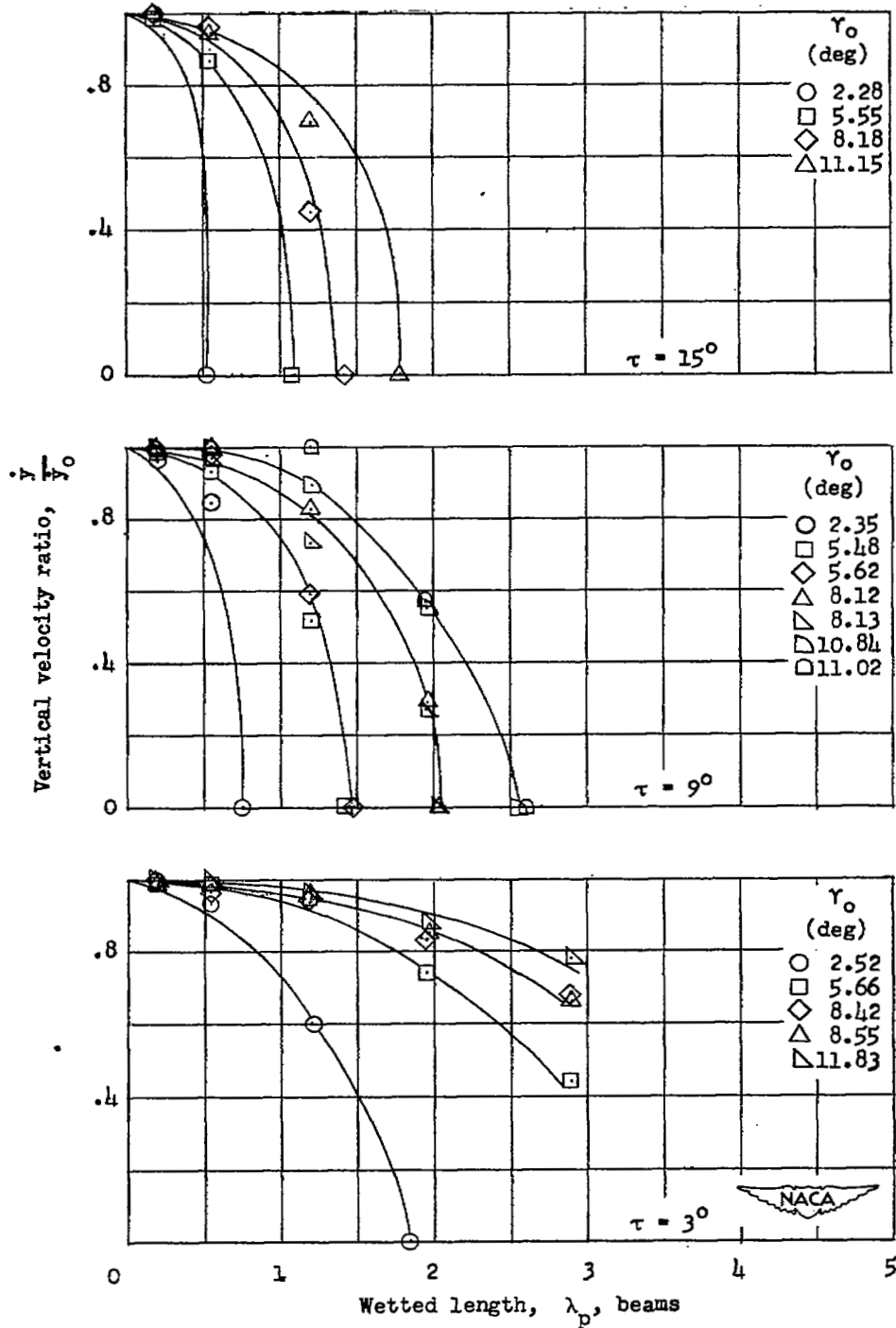


Figure 11.- Variation of vertical velocity ratio with wetted length for various trims. $C_{\Delta} = 4.4$.

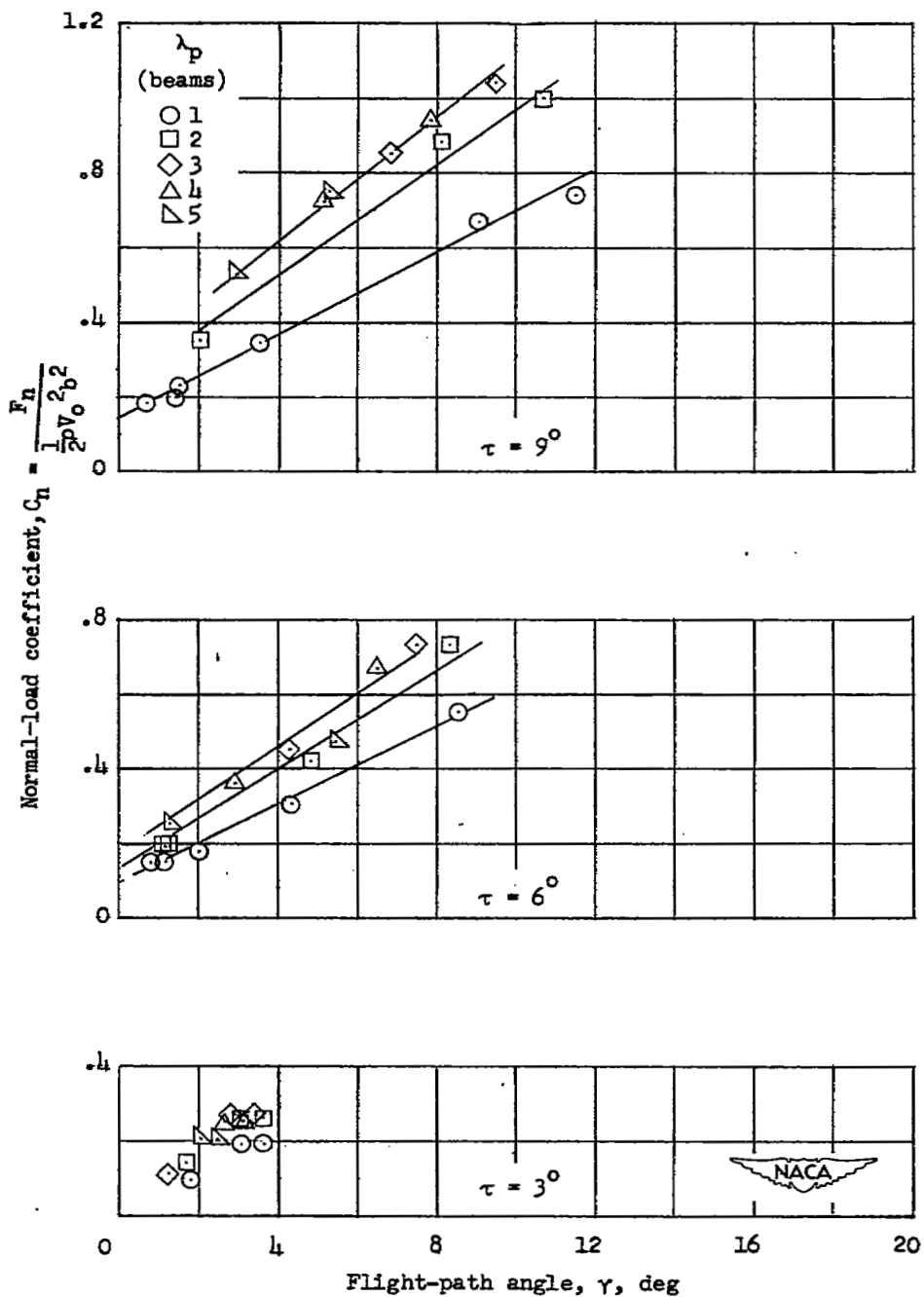


Figure 12.- Variation of normal-force coefficient with instantaneous flight-path angle for various aspect ratios. $C_{\Delta} = 18.9$.

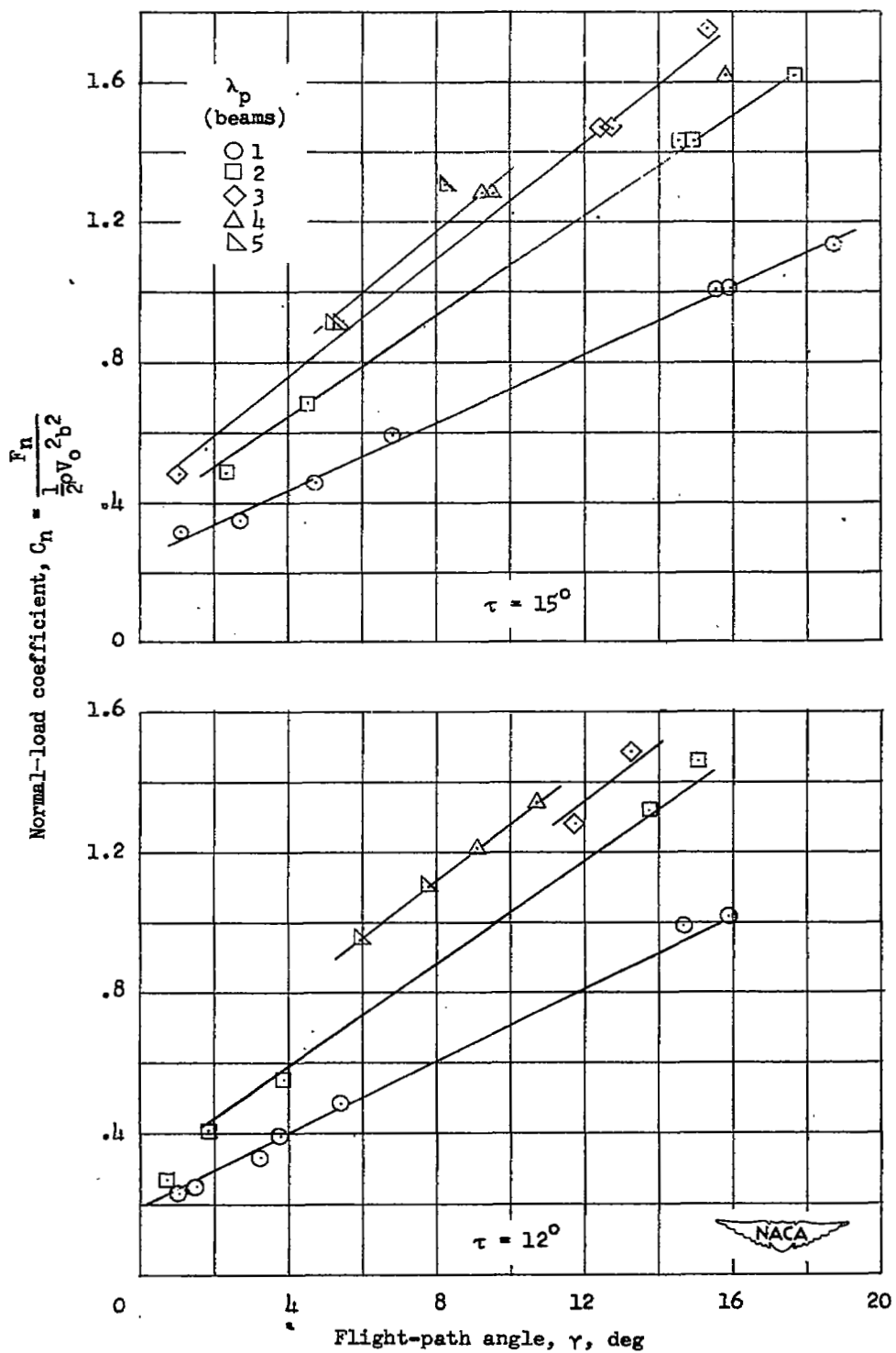


Figure 12.- Concluded.

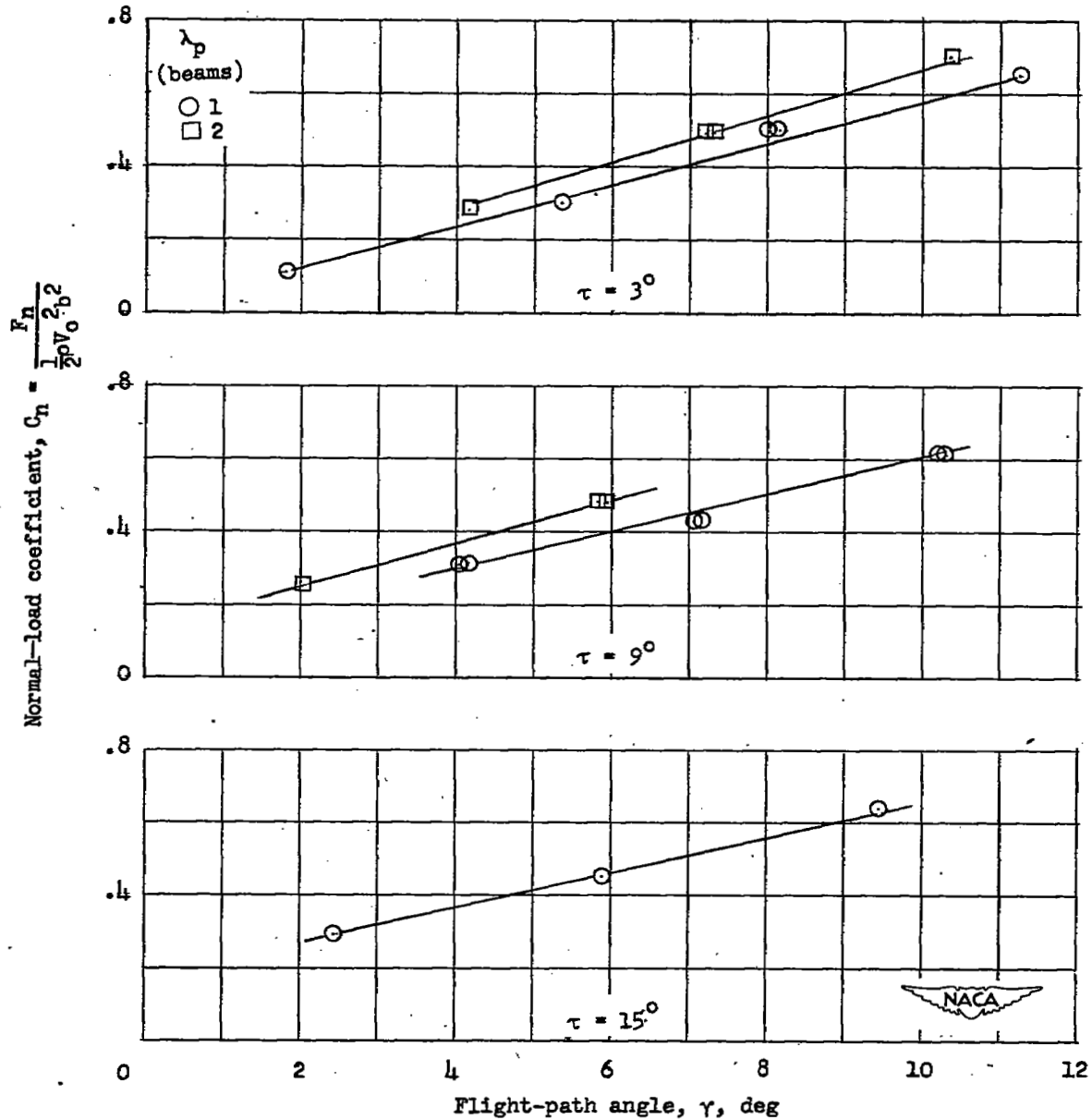


Figure 13.- Variation of normal-force coefficient with instantaneous flight-path angle for various aspect ratios. $C_{\Delta} = 4.4$.

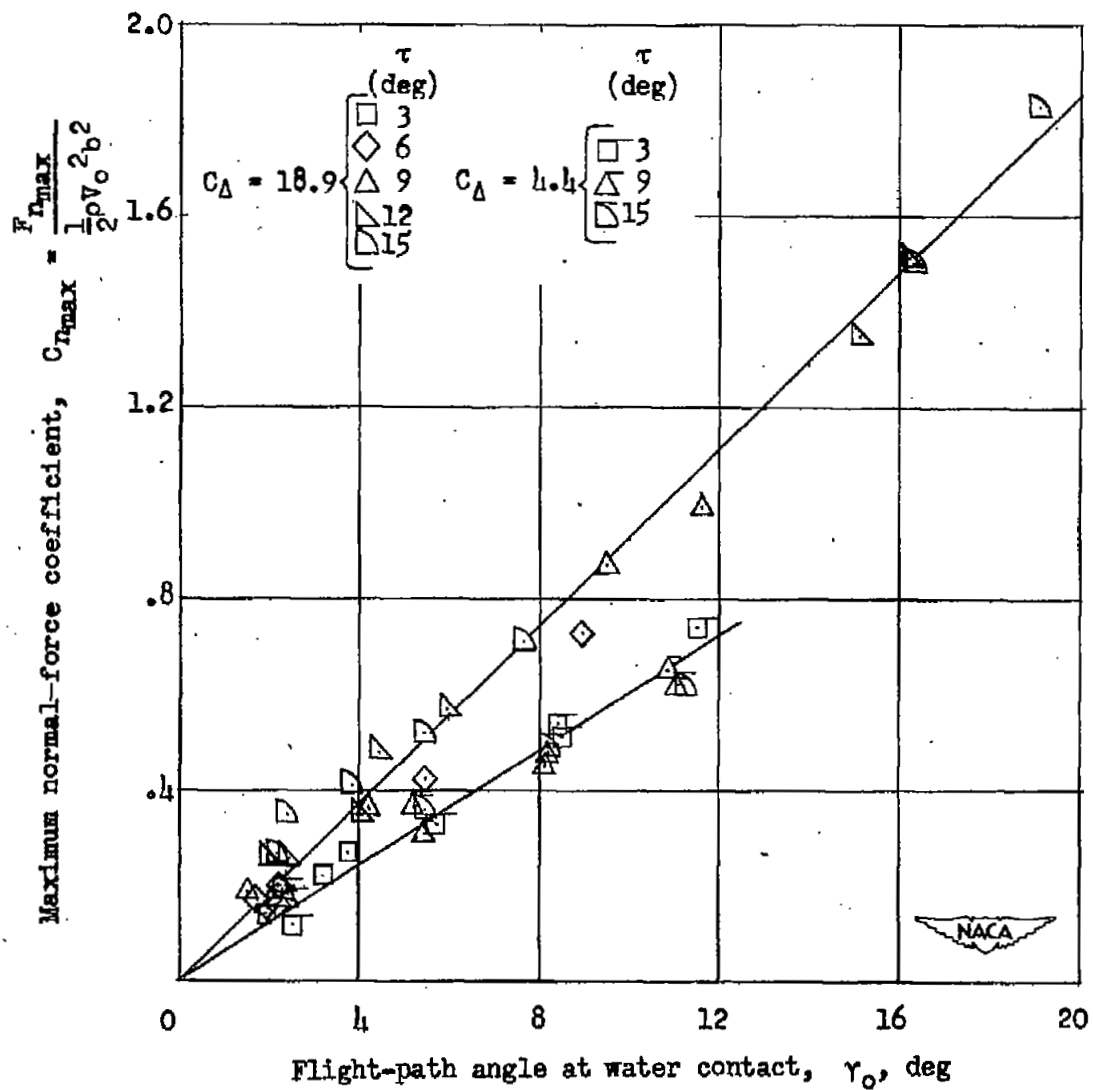


Figure 14.- Variation of normal-force coefficient at instant of maximum normal force with flight-path angle at water contact.

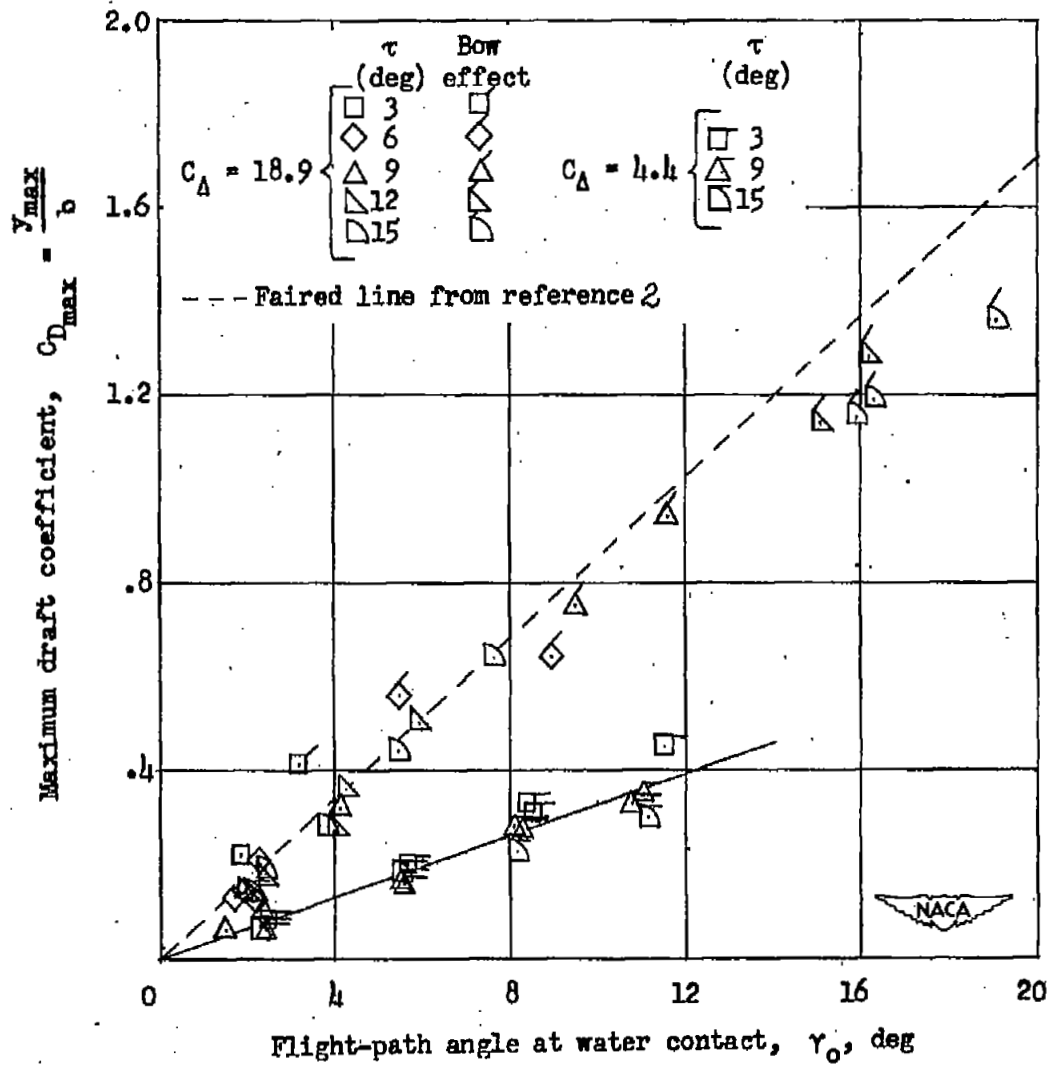


Figure 15.- Variation of draft coefficient at the instant of maximum immersion with flight-path angle at water contact.

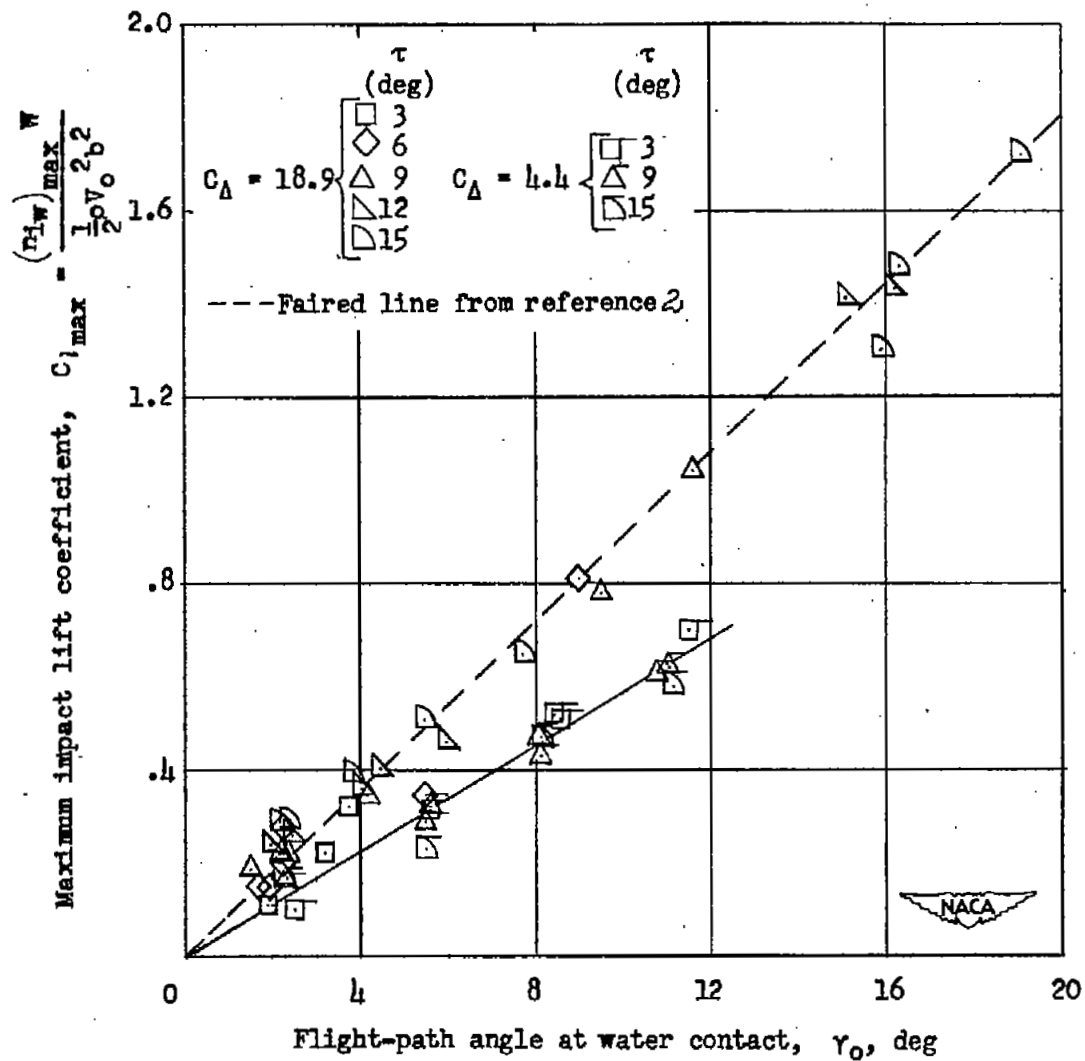


Figure 16.- Variation of impact lift coefficient at instant of maximum acceleration with flight-path angle at water contact.

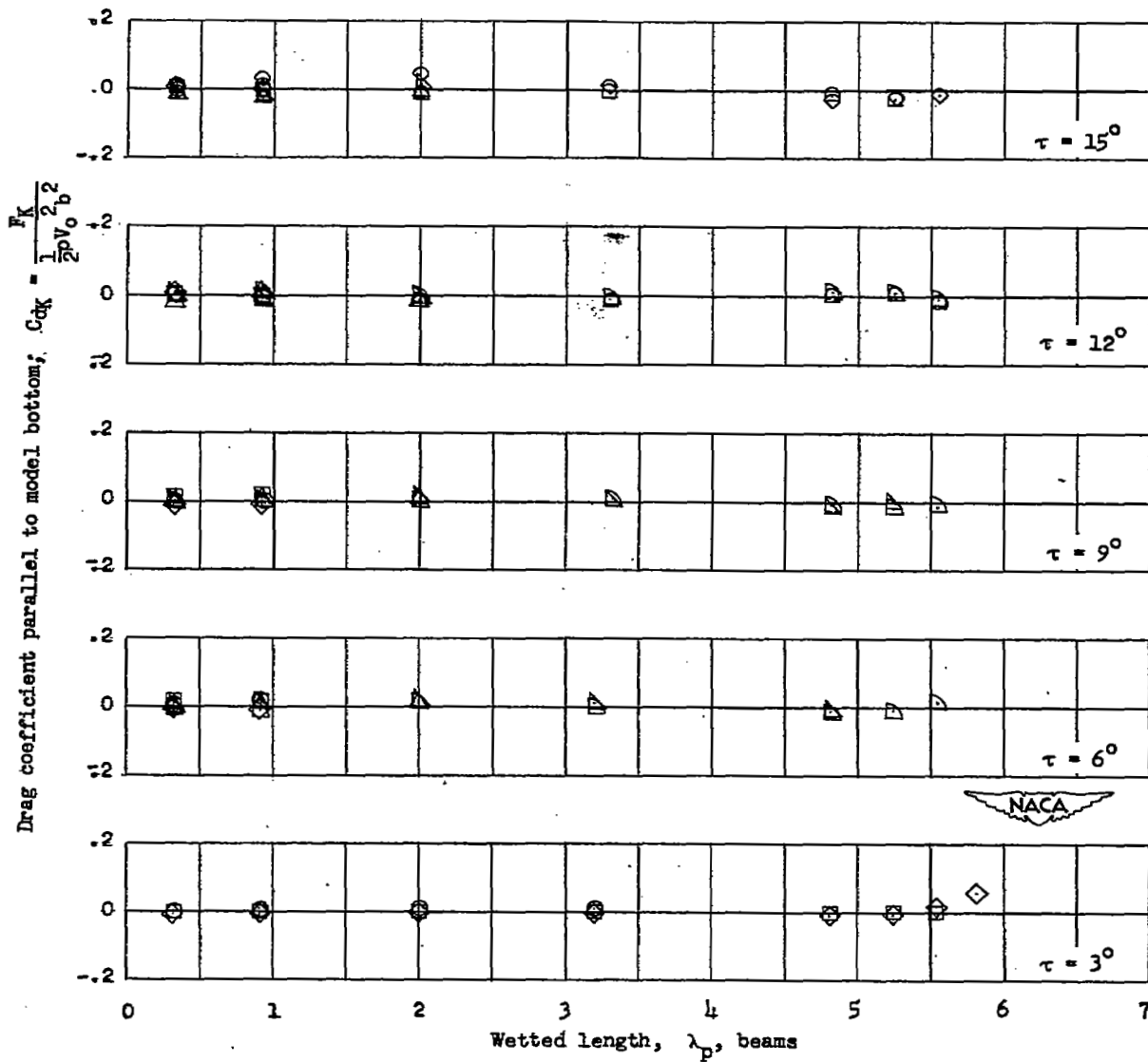


Figure 17.- Variation of drag coefficient parallel to model bottom with wetted length. $C_\Delta = 18.9$.

$$\tau = 3^\circ$$

Variation of pressure coefficient along model

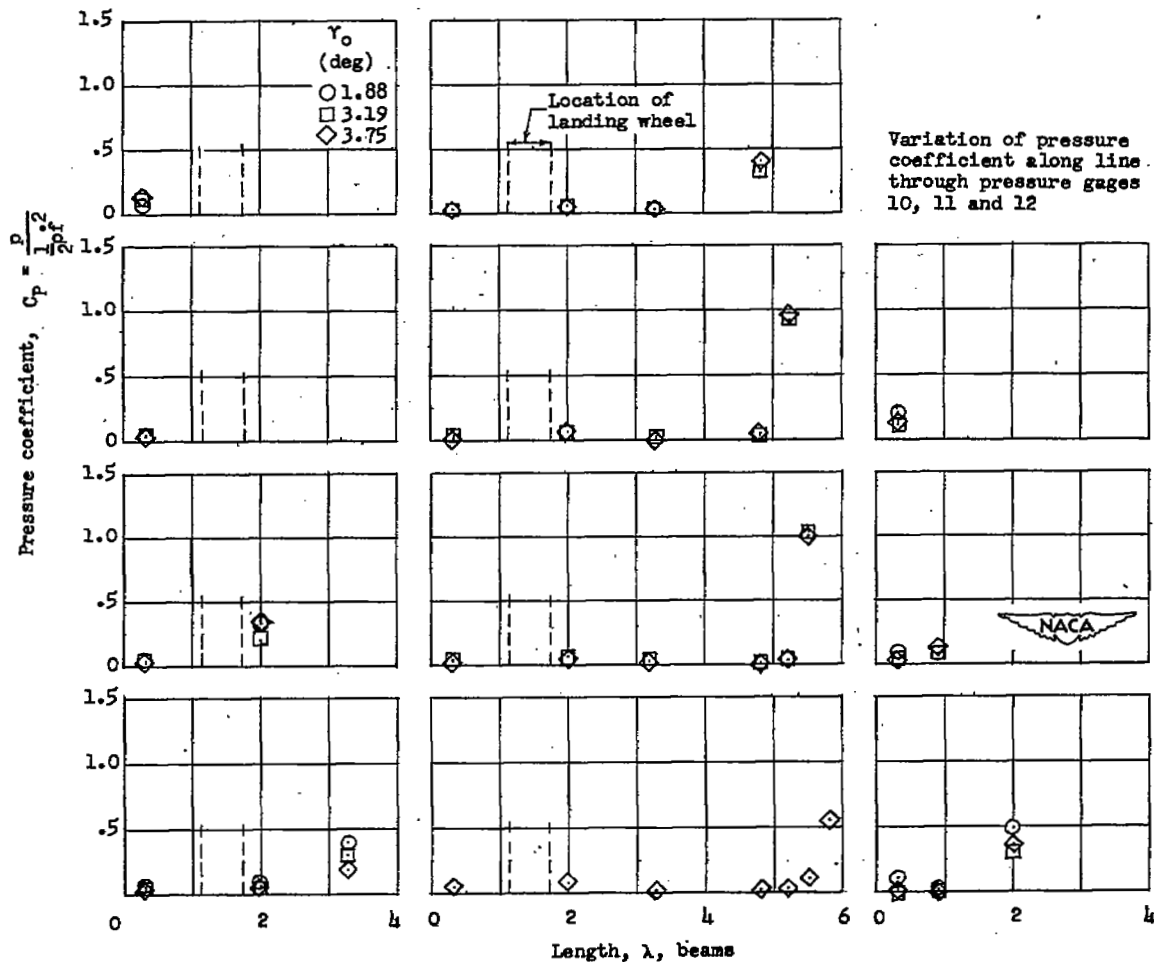


Figure 18.- Variation of bottom pressure coefficient with wetted length for various trims. $C_{\Delta} = 18.9$.

$$\tau = 6^\circ$$

Variation of pressure coefficient along model

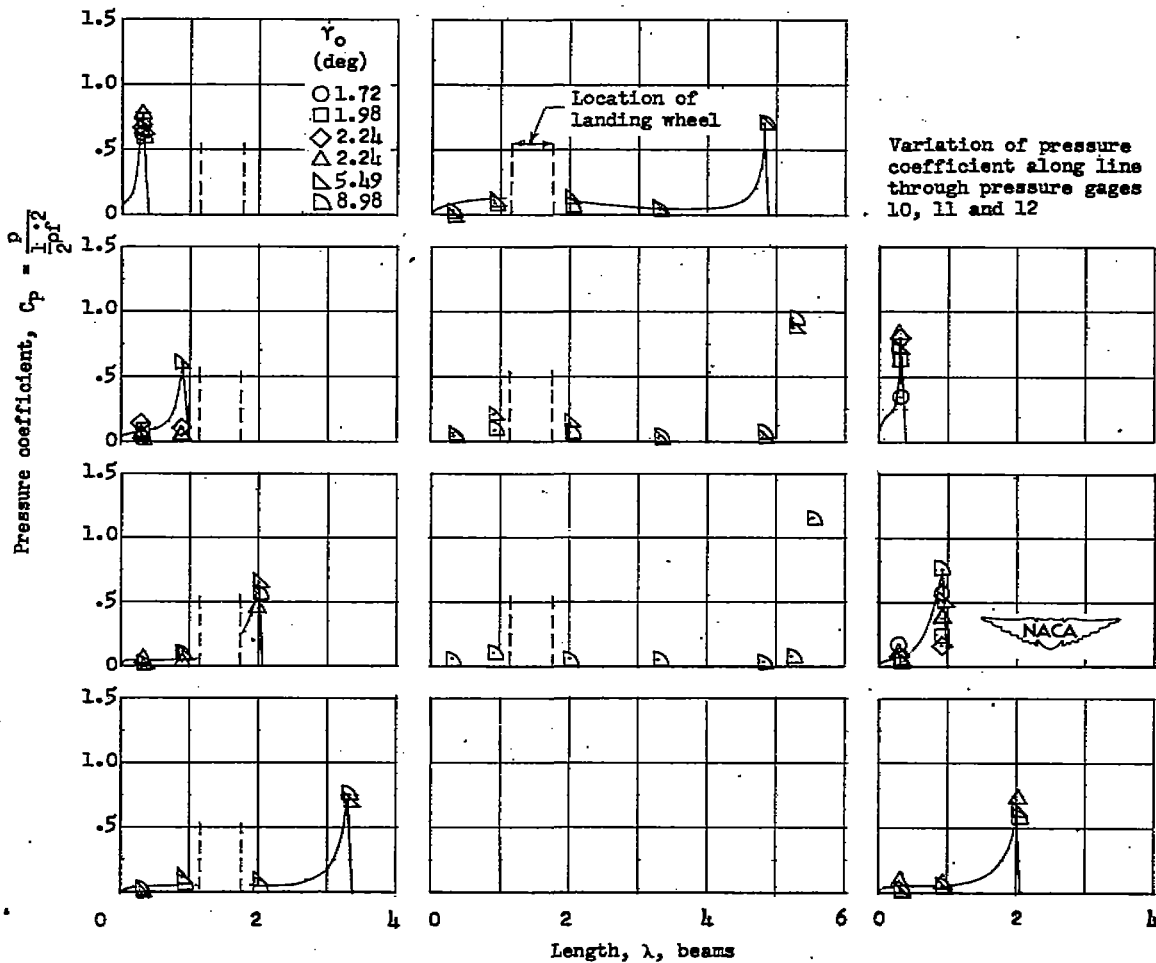


Figure 18.- Continued.

$$\tau = 9^\circ$$

Variation of pressure coefficient along model

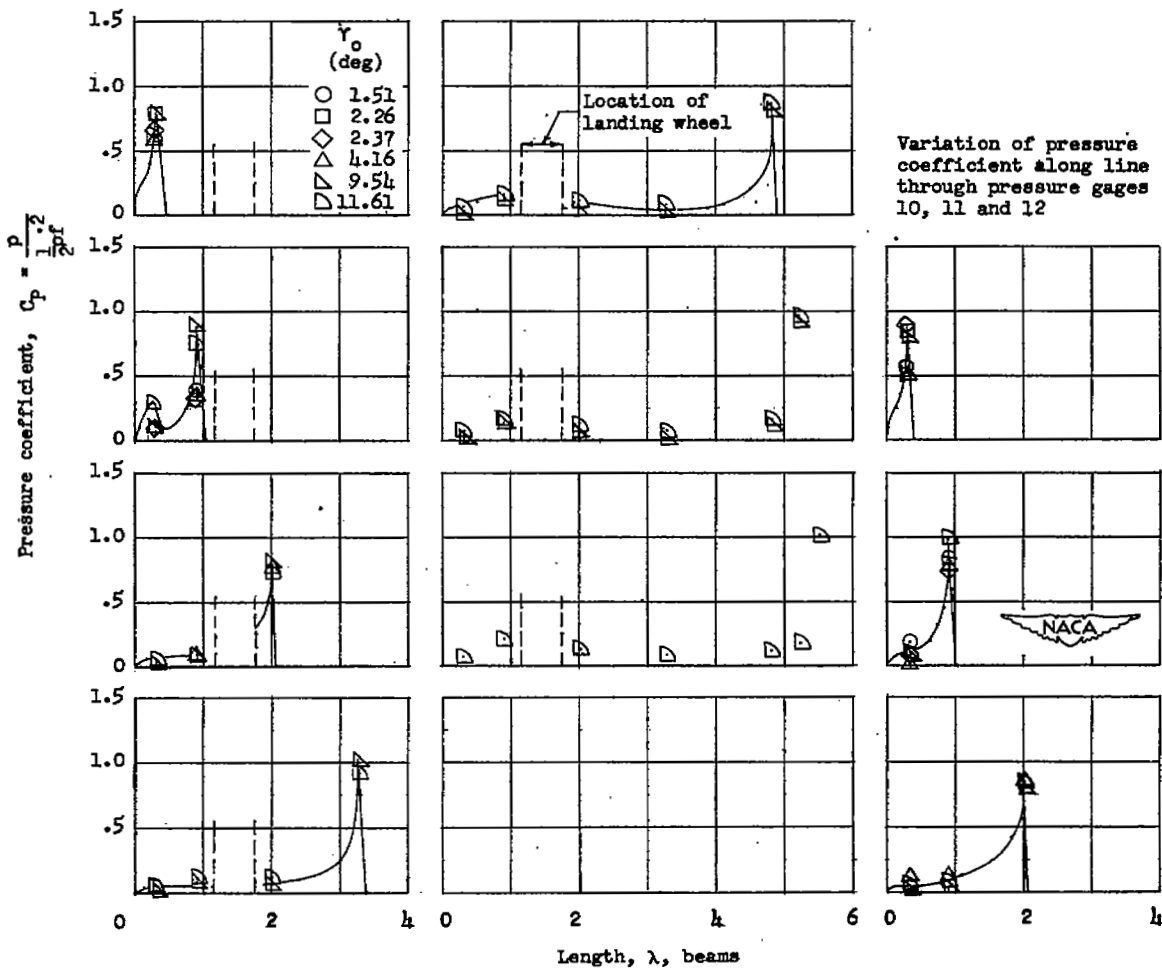


Figure 18.- Continued.

$$\tau = 12^\circ$$

Variation of pressure coefficient along model

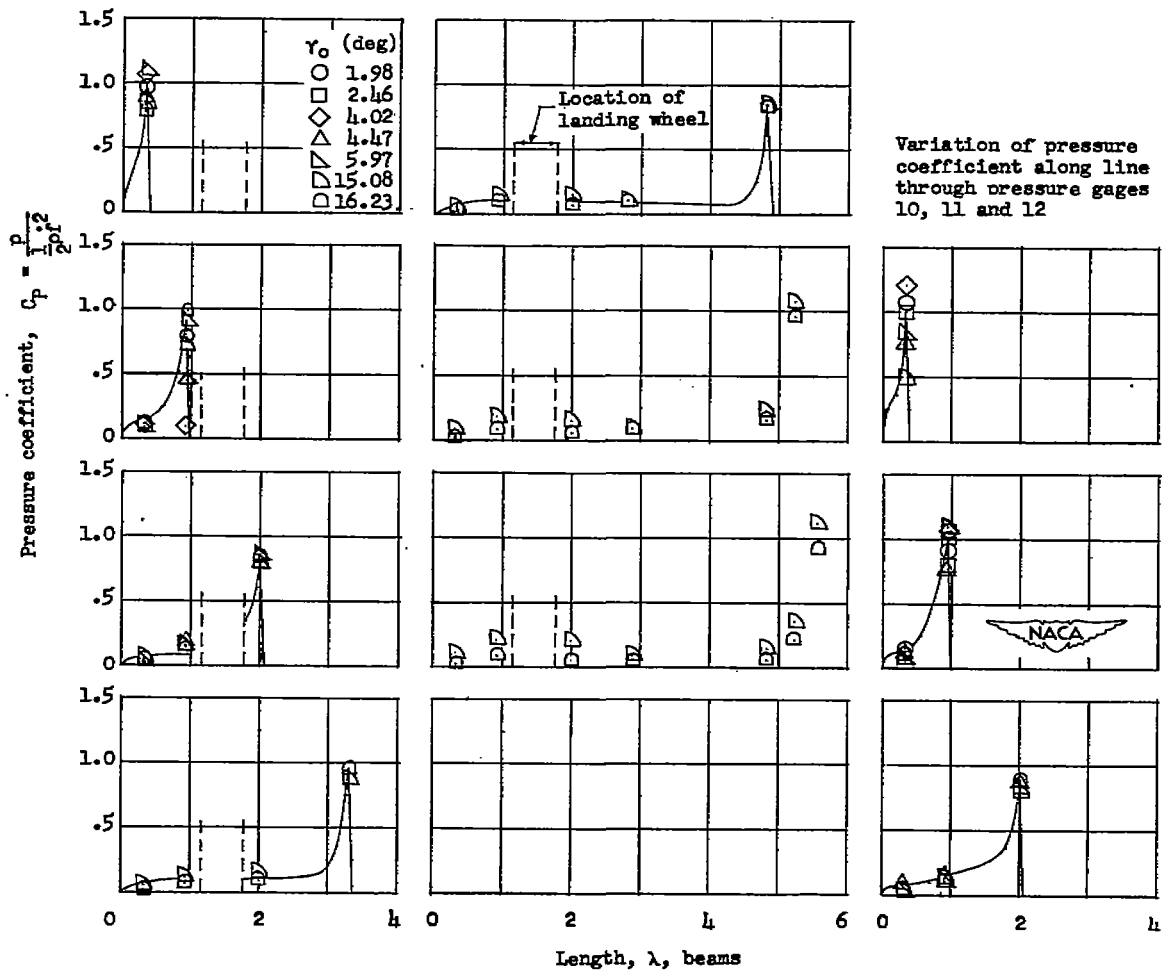


Figure 18.- Continued.

$$\tau = 15^\circ$$

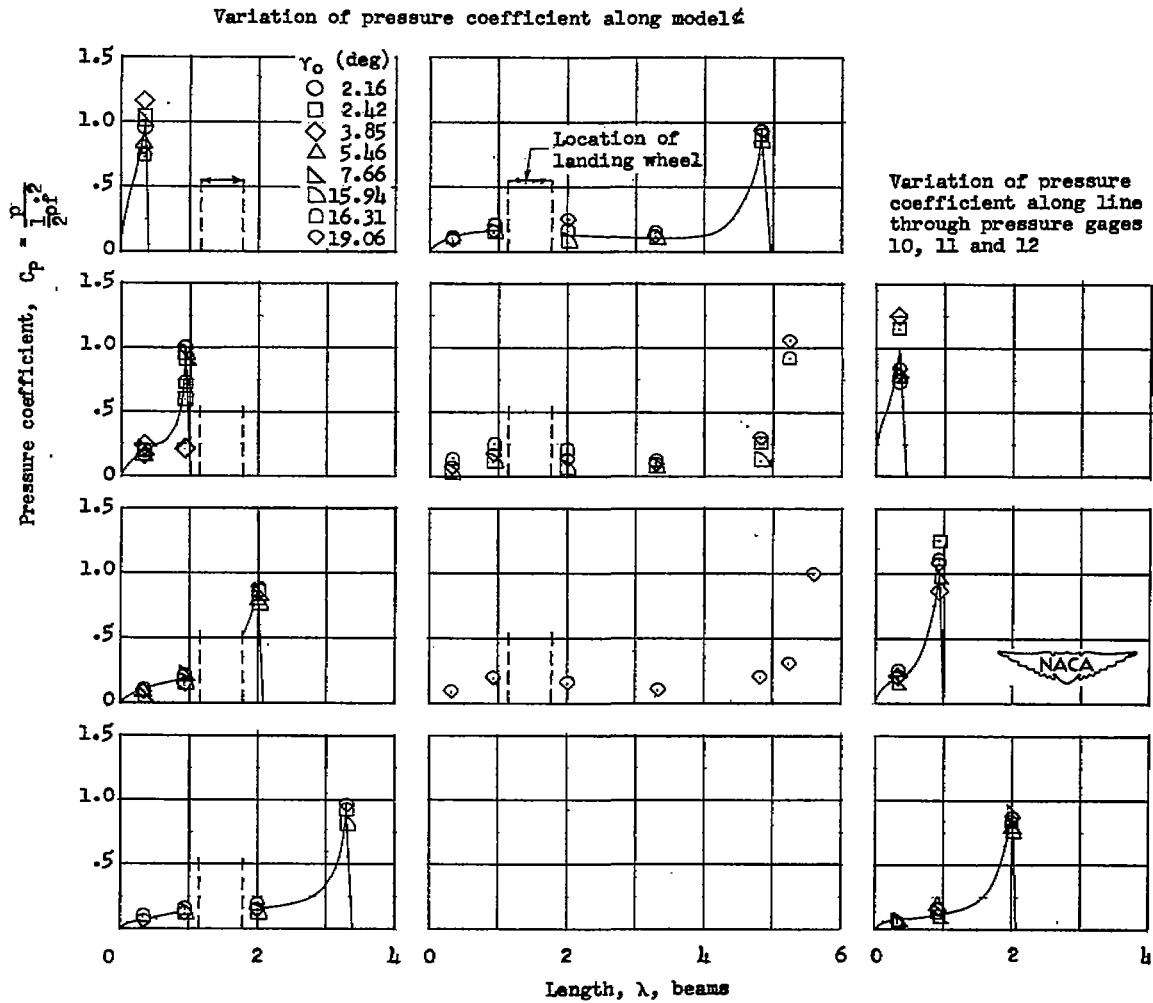


Figure 18.- Concluded.

$$\tau = 3^\circ$$

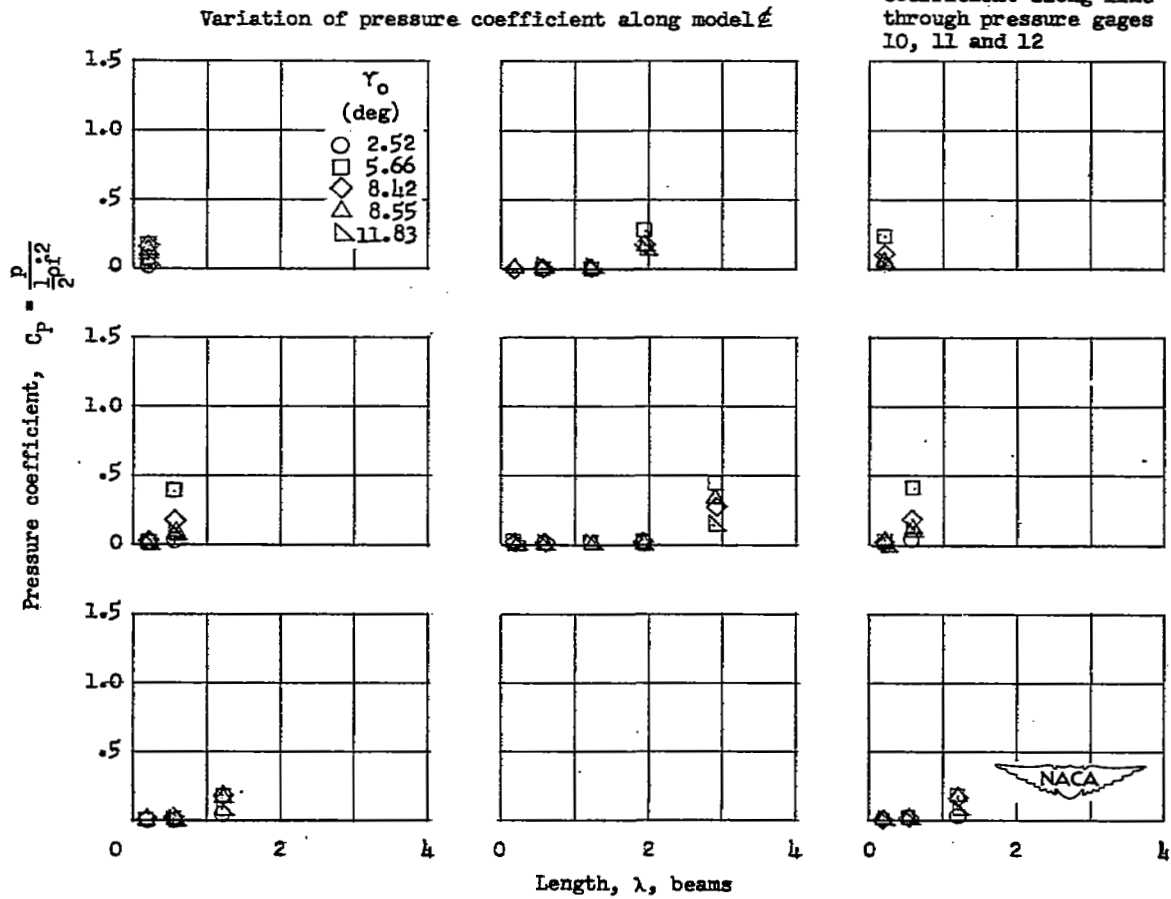


Figure 19.- Variation of bottom pressure coefficient with wetted length for various trims. $C_{\Delta} = 4.4$.

$$\tau = 9^\circ$$

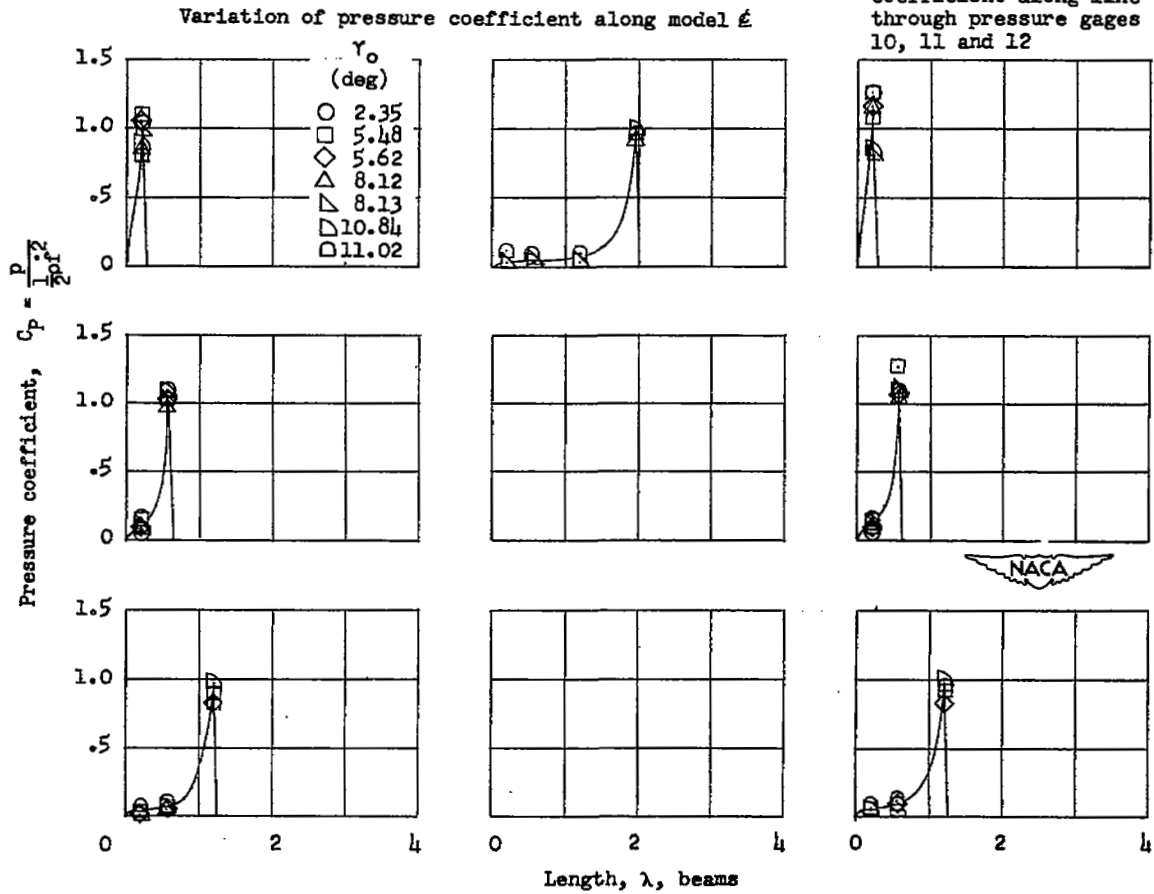


Figure 19.- Continued.

$\tau = 15^\circ$

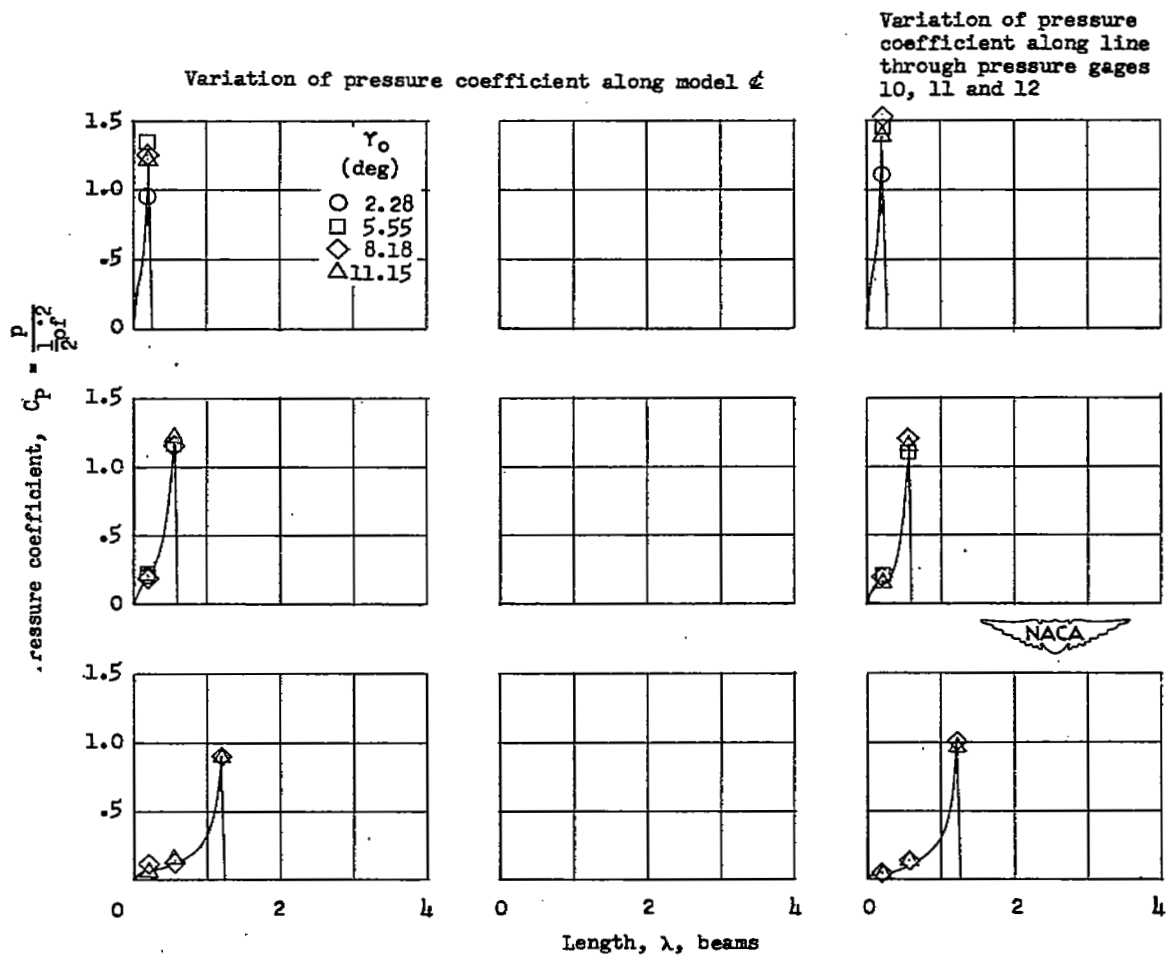


Figure 19.- Concluded.

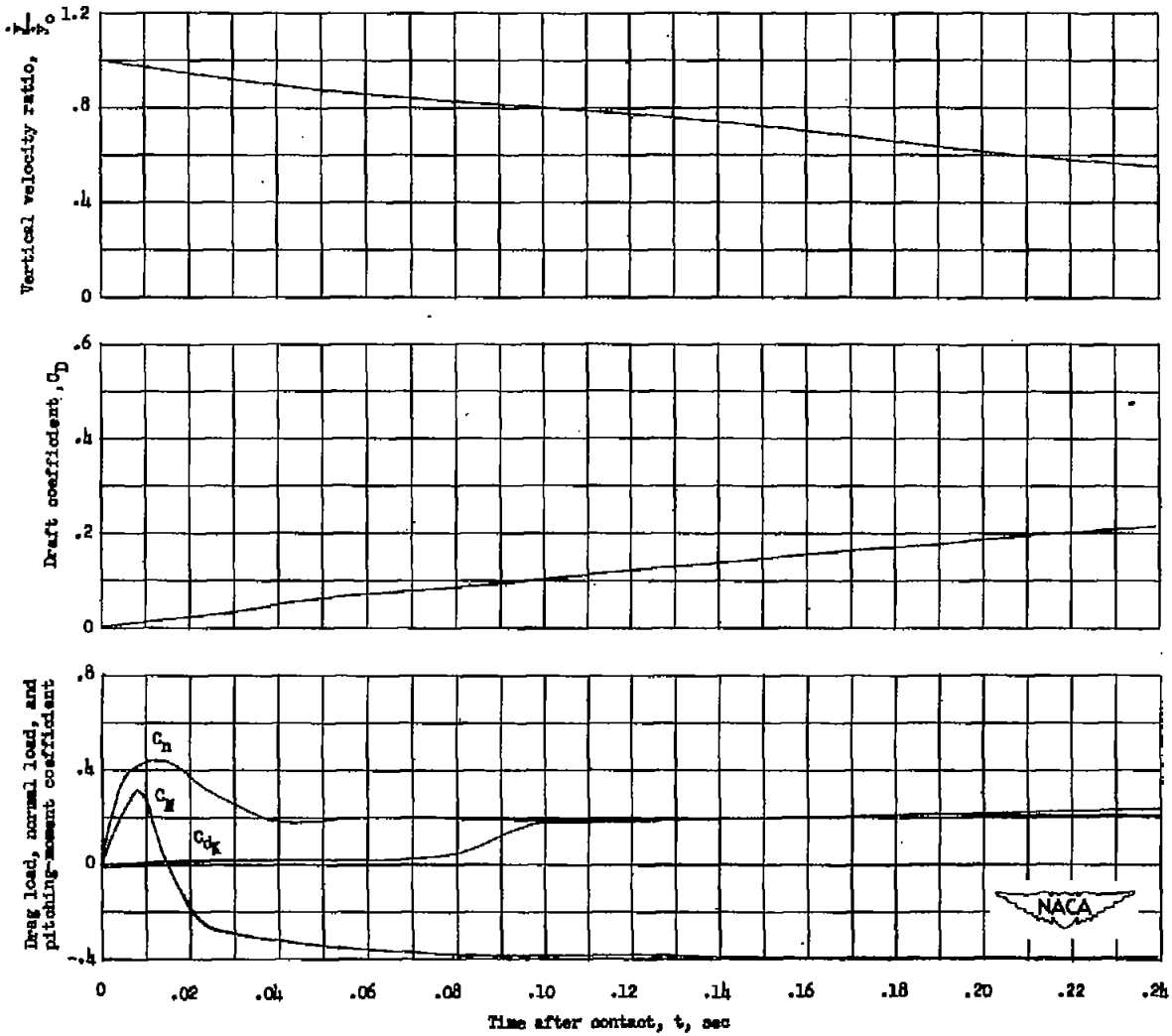


Figure 20.- Time history of loads and motions obtained during smooth-water impact at 0° trim. $C_{\Delta} = 18.9$.

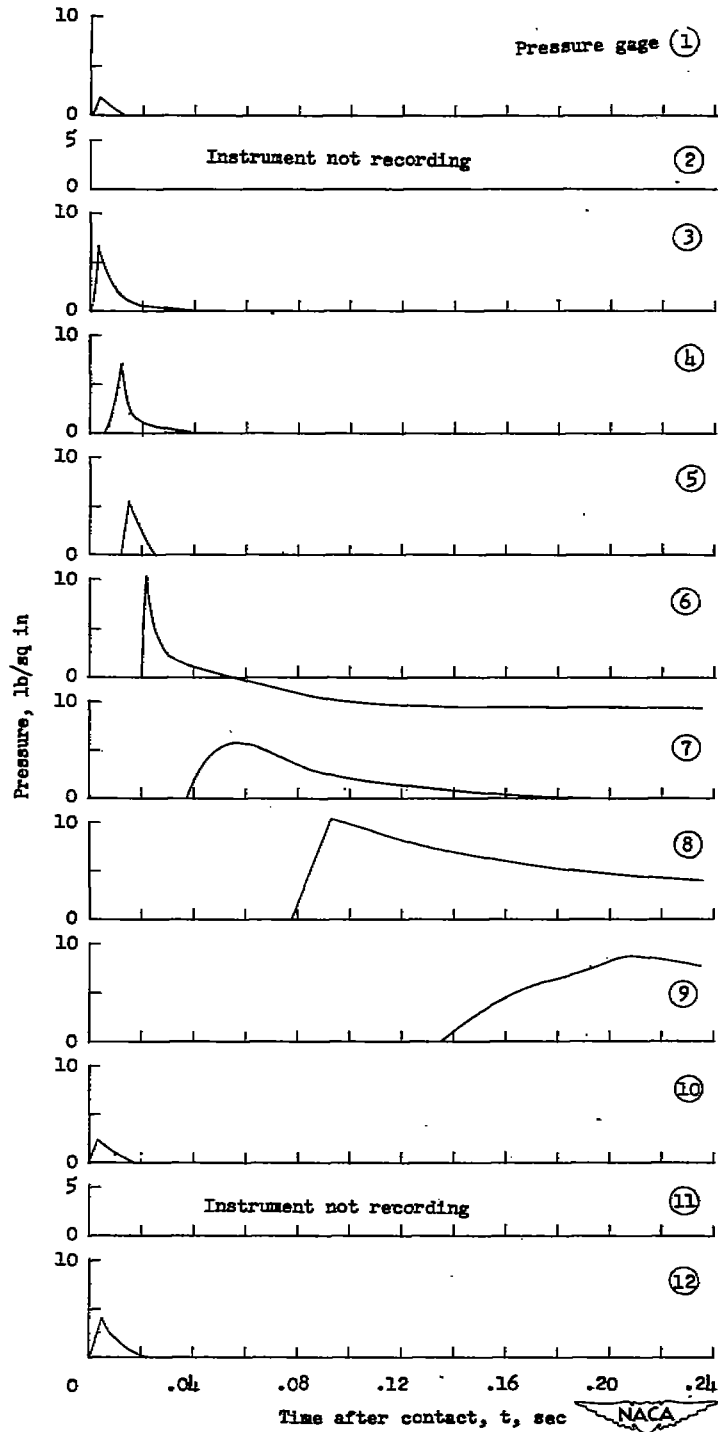


Figure 21.- Time history of unit bottom pressures obtained during smooth-water impact at 0° trim. $C_\Delta = 18.9$.

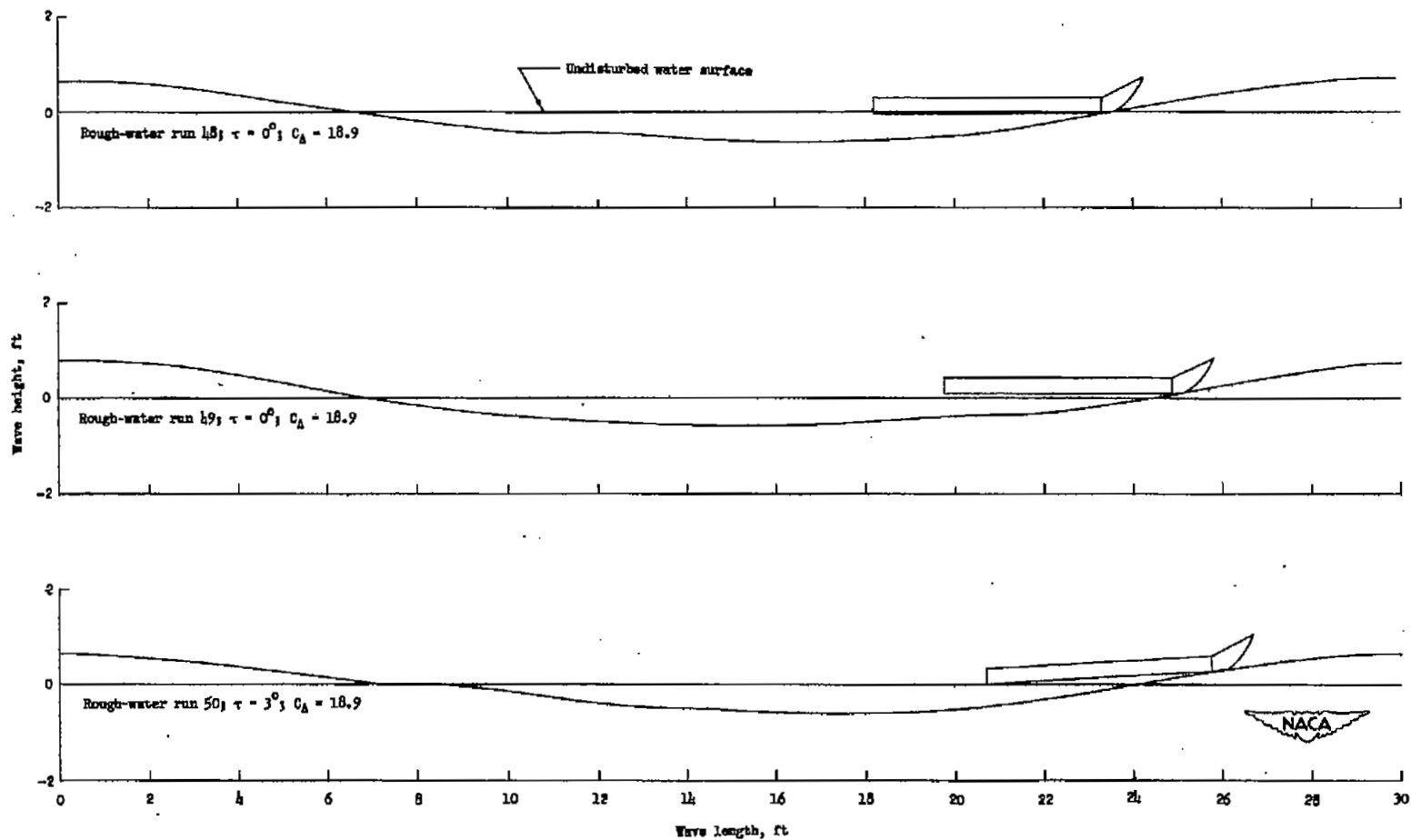


Figure 22.- Variation of wave height with wave length and initial contact location of the model on the wave for rough-water runs 48, 49, and 50.

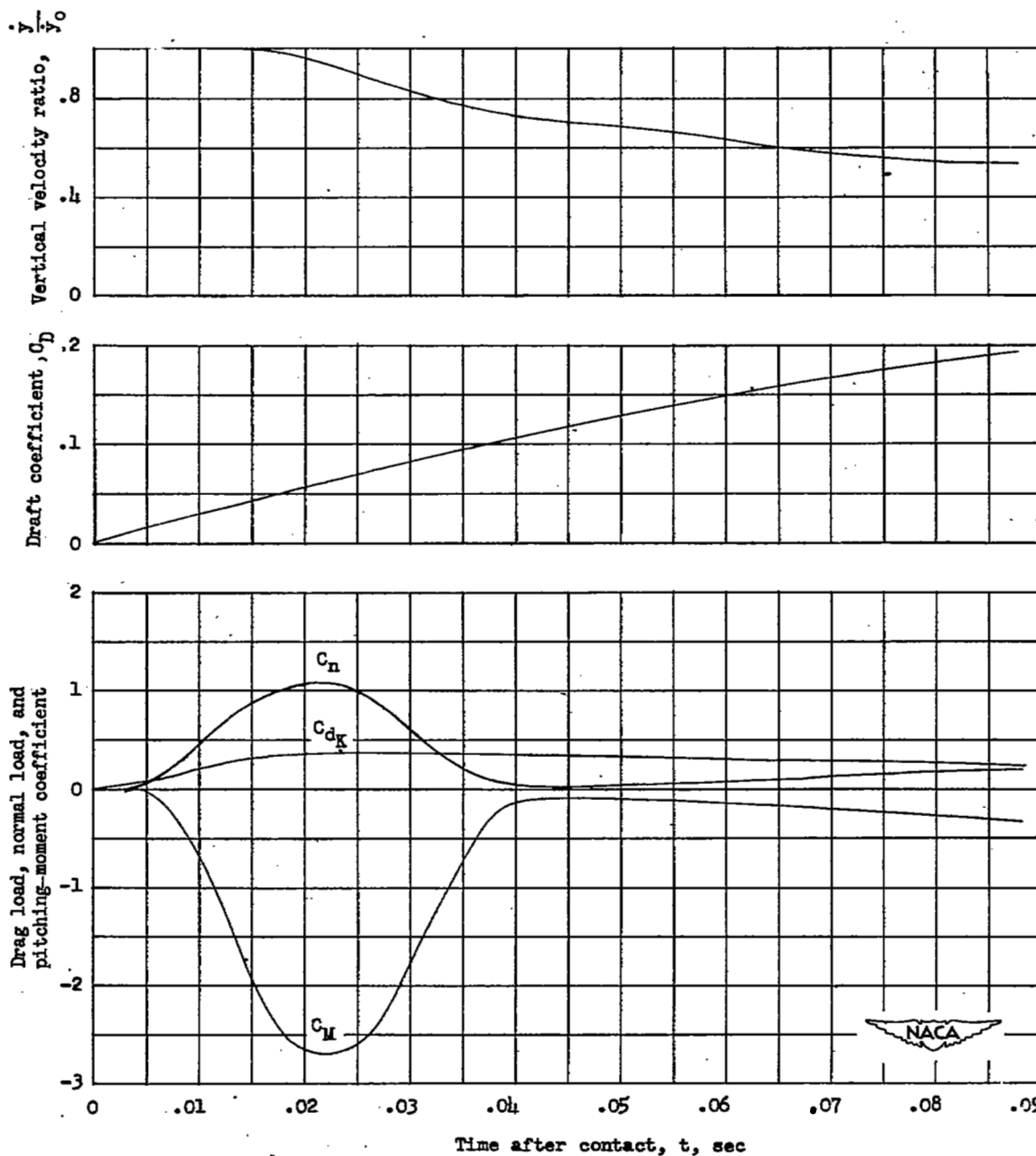


Figure 23.- Time history of loads and motions obtained during rough-water run 48 at 0° trim. $C_{\Delta} = 18.9$.

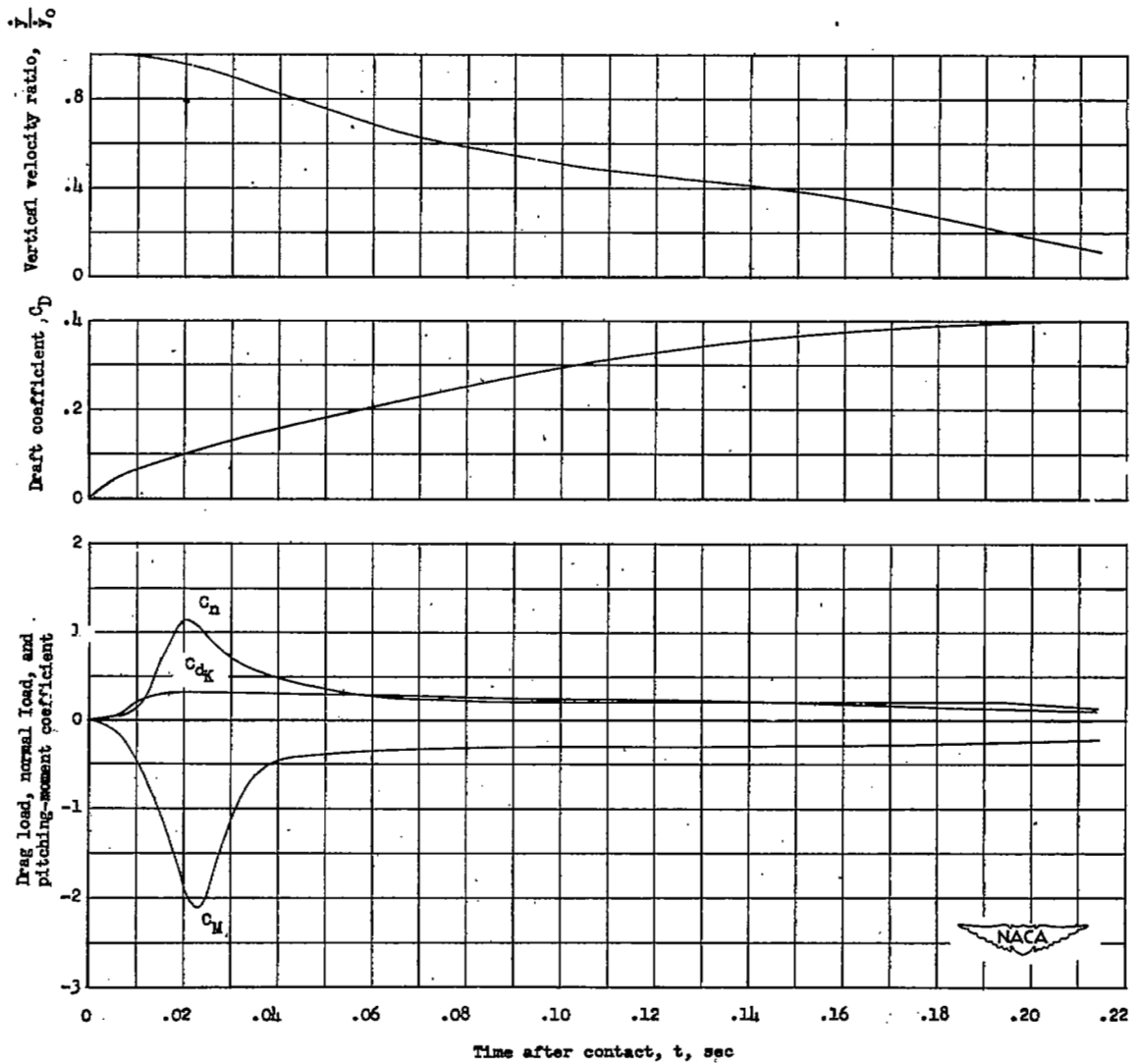


Figure 24.- Time history of loads and motions obtained during rough-water run 49 at 0° trim. $C_{\Delta} = 18.9$.

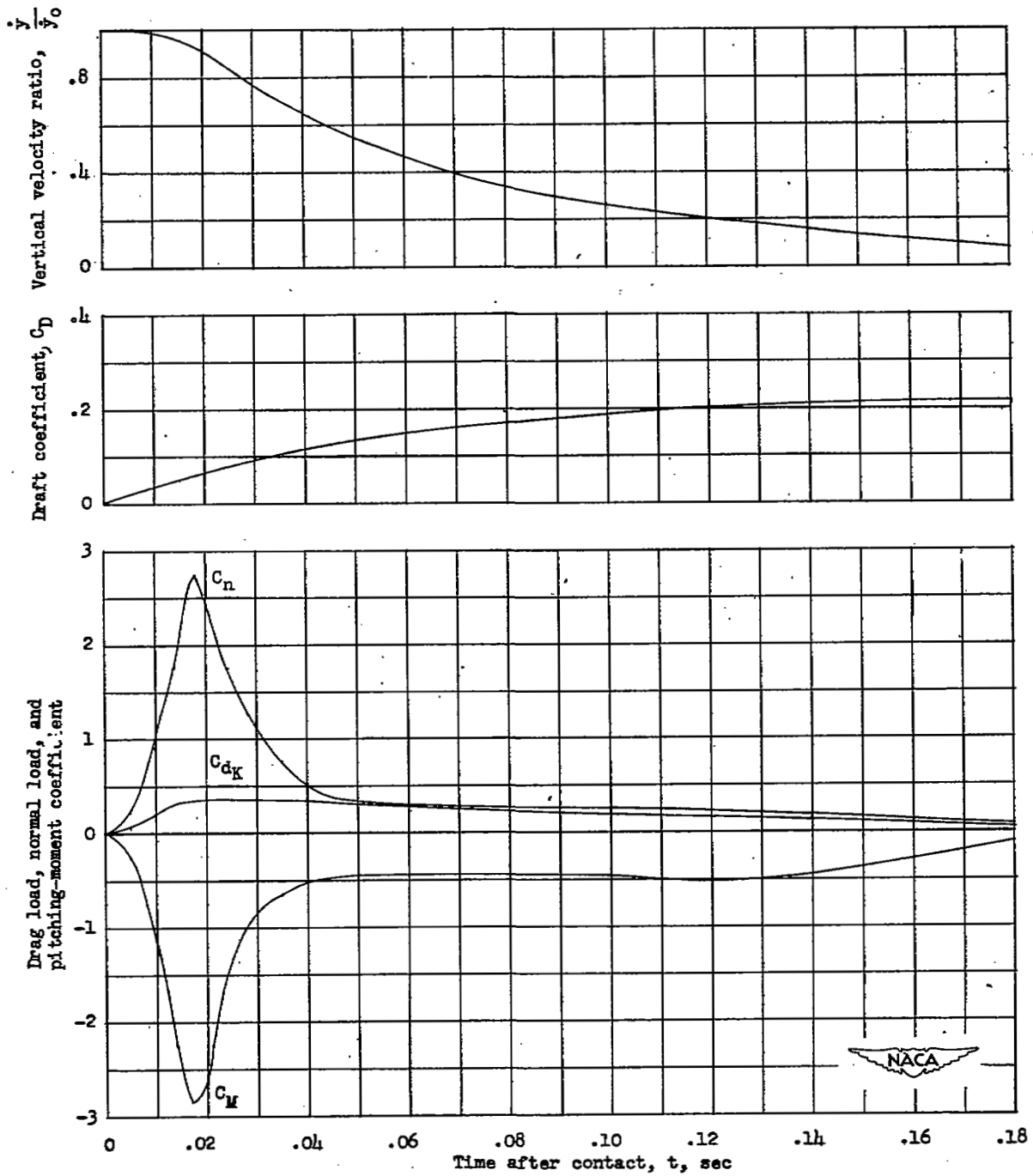


Figure 25.- Time history of loads and motions obtained during rough-water run 50 at 3° trim. $C_\Delta = 18.9$.

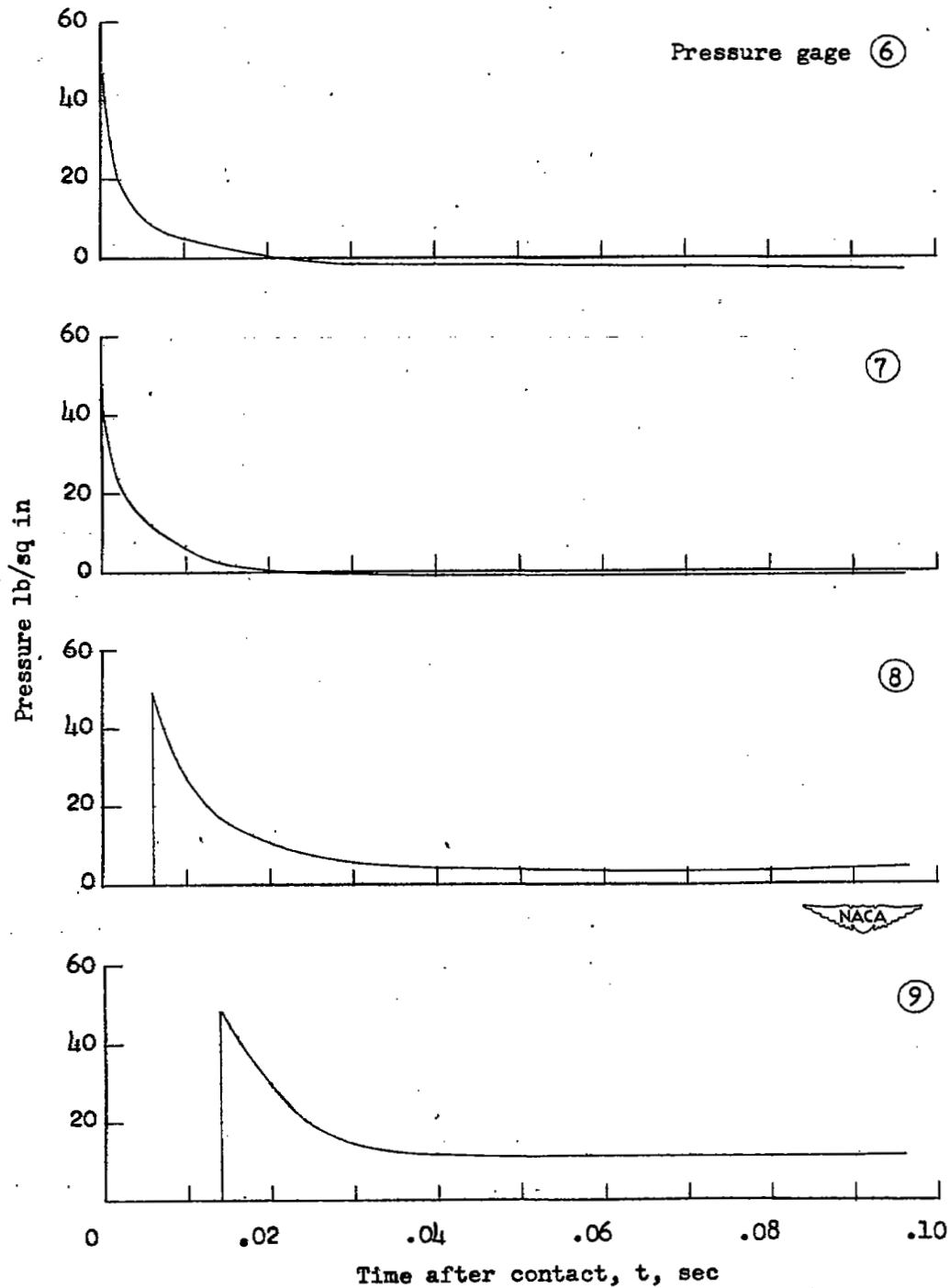


Figure 26.- Time history of unit bottom pressures obtained during rough-water run 48 at 0° trim. $C_\Delta = 18.9$.

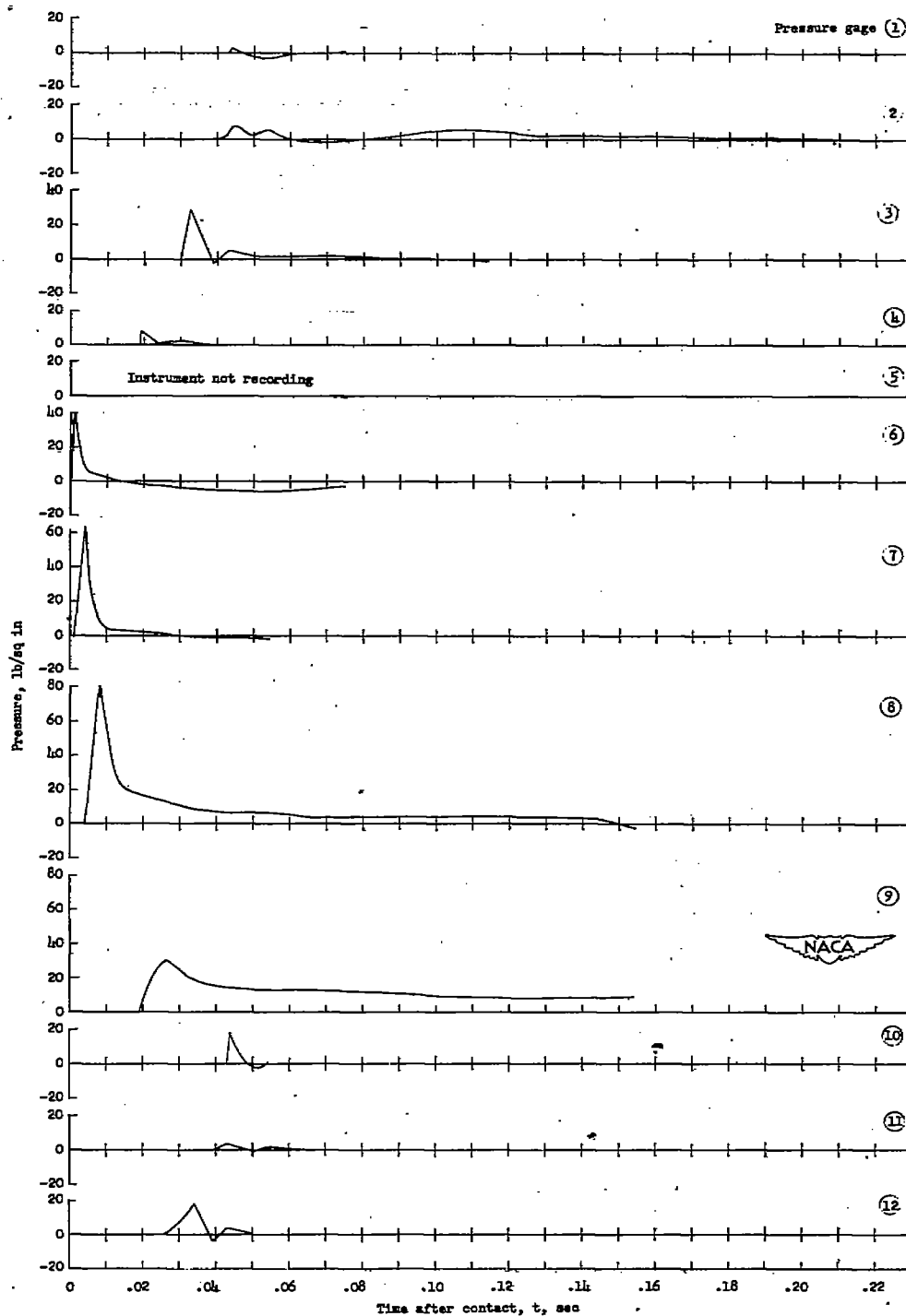


Figure 27.- Time history of unit bottom pressures obtained during rough-water run 49 at 0° trim. $C_{\Delta} = 18.9$.

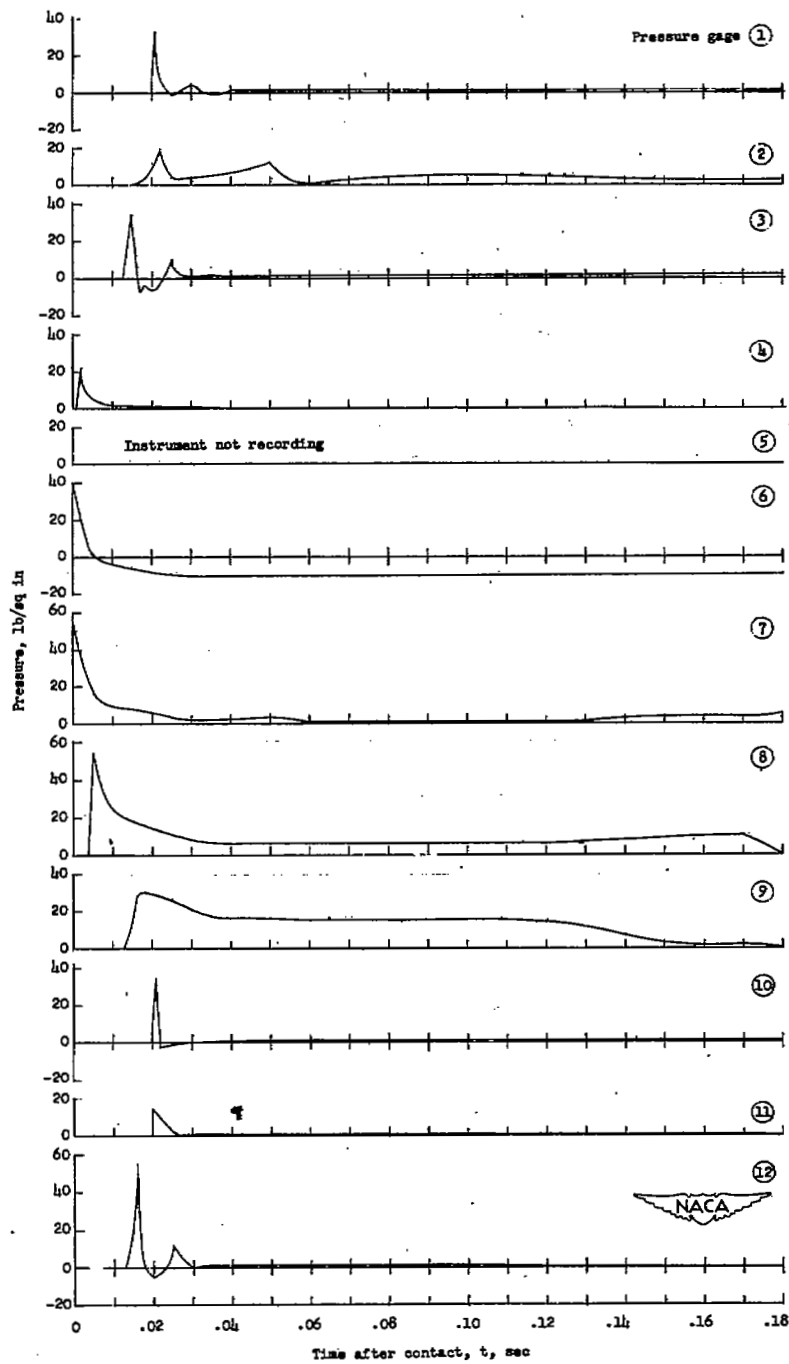


Figure 28.- Time history of unit bottom pressures obtained during rough-water run 50 at 3° trim. $C_{\Delta} = 18.9$.

NASA Technical Library



3 1176 01436 8733

